Applied Geochemistry 191 (2025) 106512

Contents lists available at ScienceDirect

Applied Geochemistry

journal homepage: www.elsevier.com/locate/apgeochem

Selectivity of tris complexation for Ni(II), Co(II), and Fe(II) and its effect on carbonate precipitation under alkaline conditions

J.L. Houghton [a,*], J.M. Haywood [a], Y. Wang [b], Y.S. Jun [b], D.A. Fike [a]

[a] Department of Earth and Planetary Sciences, Washington University in St. Louis, St. Louis, Missouri, 63130, United States
[b] Department of Energy, Environmental & Chemical Engineering, Washington University in St. Louis, St. Louis, Missouri, 63130, United States

ARTICLE INFO

Keywords:
Critical elements
Tris
Carbonates
Rosasite
Organometallic complex

ABSTRACT

Simultaneous critical element recovery and ex-situ carbon mineralization of low-grade ultramafic deposits have garnered increasing interest. Understanding the selectivity of metal complexing organic ligands for various divalent metals present in ultramafic rocks during carbonate mineralization is required to optimize this process. Here we evaluate 2-amino-2-(hydroxymethyl)-1,3-propanediol (i.e., Tris) as a model for bidentate ligands that bind divalent metals with both amine and alcohol groups in alkaline conditions (pH 8–10.5) at 25 °C and 80 °C in carbonate-buffered solutions. Protonated Tris forms a stronger complex with metal ions and is selective for trace metals with Ni(II) > Co(II) > Fe(II) during carbonate precipitation, with the rates decreasing but selectivity increasing at lower temperature and lower pH. At 25 °C, metastable amorphous hydrated carbonates form, regardless of the amount of Tris present or pH values. At 80 °C and pH 8, the Co and Fe carbonates that form are a mixture of rosasite-group minerals ($Co_2CO_3(OH)_2(H_2O)$ and $Fe_2CO_3(OH)_2$) and pure carbonates (sphaerocobaltite: $CoCO_3$ and siderite: $FeCO_3$), with the latter more stabilized with increasing Tris concentration. In mixed metal solutions without Tris at 25 °C where Fe:Ni or Fe:Co is 2:1, Fe increases the rates of Ni or Co carbonate precipitation. However, with increasing Tris concentration the presence of Ni or Co inhibits Fe carbonate precipitation. At 80 °C without Tris, Ni or Co substitute into the iron chukanovite ($Fe_2CO_3(OH)_2$) lattice, increasing Ni or Co carbonate precipitation rates. Increasing Tris concentration only slightly inhibits Fe and Co precipitation, but slows Ni precipitation up to 10 times, with Fe progressively partitioning into more pure carbonate phases with distinct crystalline morphologies. These findings suggest bidentate amine-bearing ligands may be effective at Ni and Co recovery during carbon mineralization of Fe-bearing ultramafic deposits at relatively low temperatures and slightly alkaline pH.

1. Introduction

The increasing demand for critical elements, such as Ni and Co, has led to a search for more efficient metal extraction techniques that are effective even on lower grade ultramafic deposits (Senior and Thomas, 2005; Wang et al., 2021; Matus et al., 2020; Hamilton et al., 2020). In the field of extractive metallurgy, organic metal complexing or metal chelating compounds have been evaluated for use in industrial mineral processing (see review in Lazo et al., 2017). Recent studies have focused on utilizing organic ligands to aid in recovering critical elements (Ni, Co, Fe) released during ligand-promoted silicate dissolution of laterite ores (Kursunoglu and Kaya, 2015) or serpentine minerals (Khan et al., 2021). Organic ligands promote chemical weathering of silicates both by complexing metals at the mineral surface—scavenging electrons from the metal-O bond and releasing H_4SiO_4 into solution—and by complexing the metals in solution, driving the concentrations of free metal ions down and promoting further dissolution (Prigiobbe and Mazzotti, 2011; Olsen and Rimstidt, 2008). Recent studies of ultramafic mineral dissolution have also shifted from studies of natural weathering processes towards either ex-situ or in-situ enhancement of chemical weathering as a method of carbon capture and storage (Hänchen et al., 2006; Gerdemann et al., 2007; Krevor and Lackner, 2009; Prigiobbe and Mazzotti, 2011; Sissmann et al., 2013; Bobicki et al., 2015; Snæbjörnsdóttir et al., 2020). The role of organic ligands in promoting chemical weathering has been evaluated extensively (Huang and Keller, 1972; Drever and Stillings, 1997). Early work by Grandstaff (1986)

* Corresponding author.
E-mail addresses: jhoughton@wustl.edu (J.L. Houghton), haywoodj@wustl.edu (J.M. Haywood), w.ying@wustl.edu (Y. Wang), ysjun@wustl.edu (Y.S. Jun), dfike@wustl.edu (D.A. Fike).

https://doi.org/10.1016/j.apgeochem.2025.106512
Received 7 April 2025; Received in revised form 27 June 2025; Accepted 27 July 2025
Available online 28 July 2025

demonstrated a 10-fold increase in dissolution rate of olivine in the presence of oxalate or ethylene diamine tetraacetic acid (EDTA) at pH 3.5–4.5 and 25 °C. Other studies at pH 4.0–6.5 at 25 °C in air found a 6-fold increase in dissolution rates of olivine in the presence of ascorbic acid or oxalate (Wogelius and Walther, 1991; Olsen and Rimstidt, 2008, respectively). Sissmann et al. (2013) recommended that carbonation can take place under reducing conditions at circum-neutral pH. In fact, increasing pH and alkalinity during olivine dissolution does not impede the carbonation process (Sissmann et al., 2013; Gerdemann et al., 2007) provided that secondary phases (e.g., serpentine, Fe oxides, silica) do not interfere with carbonation rates (Dufaud et al., 2009; Wang and Giammar, 2013; see review in Sissmann et al., 2013). Thus, the use of organic ligands in selective critical element recovery under conditions that facilitate simultaneous carbon storage requires an understanding of the mechanisms and relative rates of metal-ligand exchange.

The primary cations in mafic and ultramafic minerals, such as San Carlos olivine, are Mg and Fe (up to ~9 wt%), with trace metal abundances of Ni (up to ~3000 ppm) and Co (up to ~200 ppm) (Lambart et al., 2022). For the purposes of critical element recovery with simultaneous carbon storage, the optimal conditions would maximize Mg and Fe carbonate formation and minimize Ni and Co carbonate formation. The use of ligands that selectively bind reduced metals with relative strength in the order Ni ~ Co ≫ Fe would facilitate this purpose. Dioxime complexes of cobalt and nickel were used in analytical electrochemistry due to their enhanced signal compared to free Co (II) or Ni (II) ions (Baxter et al., 1998; Ma et al., 1997; Saito and Moffett, 2001) and are commonly used in applications to sequester metals *via* chelation. Dioxime and related compounds such as dimethylglyoxime complex relatively strongly with Co (II), Ni (II), and Fe (II), with the relative stability constants in order of Ni > Fe > Co (Saito and Moffett, 2001; Zhang et al., 1990; Martell et al., 1993; Jillot and Williams, 1958). However, these ligands have low solubility in water and are only stable in the presence of a reducing agent and a base, making them difficult to work with when studying conditions relevant to natural systems. EDTA is another metal chelating ligand commonly used in a wide array of industrial processes to bind metals (including Fe, Ca, and Mg) because it is water soluble and functions across a wide pH range (Fangueiro et al., 2002). However, the relative logarithm of stability constants of metal-EDTA complexes are almost identical for Co (II), Ni (II) and Fe (II) (16.4, 18.4, and 16.0, respectively; Martell et al., 1993), challenging the element separation.

Simpler compounds that form complexes with metals include citrate, oxalate, and various amines. Oxalate and citrate are common organic acids found in natural sediments with decomposing organic matter but only contain carboxylate functional groups, both of which contain weakly basic negatively charged oxygen donor groups, meaning the relative acidity of the metal ions primarily controls the strength of the complex (Hancock and Martell, 1989). In general, amine functional groups are expected to more strongly complex transition metals due to their more basic nature and, as sigma donors, are stronger field ligands than carboxylates (Stumm et al., 1996; Nieboer and Richardson, 1980). Tris (i.e., tris(hydroxymethyl)aminomethane or 2-amino-2-(hydroxymethyl)-1,3-propanediol, also known as THAM) is a synthetic molecule with similar structure to common amino acids (e.g., serine, glycine) for which metal complexation has been studied, primarily in the medical field due to its common use as a pH buffer (Kondratenko et al., 2022; Nagaj et al., 2013). During metal complexation, bonding takes place with both the amine group and one of the alcohol groups to create a bidentate complex, with complete chelation occurring if excess Tris is available (Dotson, 1972; Hall et al., 1962). The addition of a neutral oxygen donor to the binding environment means Tris will also be selective based on ion size, favoring larger metal ions, although the geometry of each complex can introduce steric strain that hinders a simple prediction of selectivity (see review in Hancock and Martell, 1989). Because Tris is a readily available, cost effective, non-toxic, water-soluble amine that is expected to also have selective complexing properties for different transition metals, it was chosen as the model molecule in this study of its selectivity of ligand exchange mechanisms and kinetic rates of carbonate formation.

The solubility of Fe(II), Ni(II) and Co(II) carbonates has been determined and predict a relative stability of Co > Fe > Ni (Smith et al., 1976; Naumov et al., 1974; Singer and Stumm, 1970; Wallner et al., 2002) although the logK_{sp} is very similar among them ($CoCO_3$(s): 9.98; $FeCO_3$(s): 10.24; $NiCO_3{\cdot}6H_2O$: 10.64, respectively). In particular, the Fe (II) carbonate mineral system has been studied extensively due to its importance in natural marine sedimentary systems (Dideriksen et al., 2015; Jiang and Tosca, 2019, 2020) and steel corrosion (Azoulay et al., 2012; Kim et al., 2017). The amorphous phases of Fe(II) carbonate formed at ambient conditions in these studies include the hydroxycarbonate chukanovite (in the rosasite group of minerals having the structure $Me_2CO_3(OH)_2(H_2O)_x$ where Me is a given metal and water can be present within the lattice) and amorphous Fe(II) carbonate (AFC). The inconsistencies in reported equilibrium constants of the other transition metal carbonates were reviewed by Grauer and Berner (1999) for the purpose of nuclear waste management, and subsequently revisited by Hummel and Curti (2003) who clarified the discrepancies in the literature and endorsed the thermodynamic study by Wallner et al. (2002) for the Ni(II) carbonates hellyerite and gaspéite. A recent study of the co-precipitation Co–Ca carbonates at ambient conditions determined the presence of Co(II) altered the final mineral product of $CaCO_3$ (favoring aragonite over calcite) and promoted the formation of a Co hydroxycarbonate of the rosasite group rather than sphaerocobaltite (González-López et al., 2018). A study of Co(II) carbonate precipitation in silica gels produced amorphous cobaltite (Katsikopoulos et al., 2008). Riechers et al. (2022) explored the competitive growth of $CoCO_3$ and Co $(OH)_2$ phases on $CaCO_3$ surfaces (Riechers et al., 2022). Interestingly, however, the behavior of these metals in mixed metal carbonate-saturated solutions is understudied, although in both natural systems and industrial settings multiple metals will almost always be present and compete for ligands in solution, thus potentially affecting the carbonate mineral that precipitates.

In this study we evaluate the effect of Tris on metal complexation and carbonate precipitation under alkaline conditions. Following the suggestions of Sissmann et al. (2013), we tested conditions more favorable for carbonate precipitation (pH 8–10.5) at relatively low temperature (25 °C and 80 °C). We target the critical elements Ni and Co in the presence and absence of Fe, to improve the predictive understanding of how primary amine ligands impact metal mobility in both natural and industrial environments. The relative rates of carbonate formation are compared in single metal and mixed metal solutions and the mineral products are characterized to determine conditions that may favor Ni and Co concentration and subsequent recovery. Determining the optimal conditions that allow Tris to selectively bind Ni and Co and prevent carbonate precipitation, particularly in the presence of Fe in solution, is necessary to promote ligand-assisted simultaneous carbonation and critical element recovery from low-grade ultramafic deposits.

2. Methods

2.1. Experimental design

Experiments were conducted anaerobically in batch using gas tight 50 mL serum bottles with butyl rubber stoppers. Stock metal solutions (60 mM $NiCl_2$, $CoCl_2$, or $FeCl_2$), Tris solutions (75 mM), and carbonate buffer solutions (HCO_3:CO_3 ratio of 20 at variable concentrations depending on the required dilution for each experiment) were made separately in deionized water purged with N_2 for at least 1 h to minimize oxidation of the metals during the experiment. To test the stability of the metal complex under different pH conditions, Tris buffer solution was prepared using a Tris-HCl:Tris base ratio of 1.3 (pH ~ 8.0) or using only Tris-HCl (pH ~ 4.7). Individual Tris-metal solutions were mixed in N_2-purged empty bottles (purged for at least 10 min) in the desired ratios

(0.25, 0.5, 1, 2, and 3). For the mixed metal experiments (2:1 Fe to Co or Ni), separate stock solutions of each metal were prepared and then mixed to the desired metal ratios prior to mixing with Tris. Each Tris-metal solution was added to individual experiment bottles containing carbonate buffer to set the final concentration of bicarbonate (100 mM), carbonate (5 mM), and the desired final metal concentration. Initial metal concentrations were set to 5 mM for single metal experiments, 3 mM for pH experiments (pH 8 to 10.5), and 1 mM Co or Ni and 2 mM Fe for metal mixture experiments. These concentrations were chosen to allow carbonate precipitation of sufficient solids for characterization by XRD and FTIR after recovery, assuming complete metal precipitation, from the 50 mL volume set by the gas-tight serum bottles. For 25 °C experiments, the experiments were conducted on the bench, with agitation just prior to sampling; for 80 °C experiments, the bottles were placed in an orbital shaker/incubator to set the constant temperature with constant agitation.

Aqueous sampling was conducted using N_2 flushed syringes and needles (to minimize oxidation) at regular intervals. If needed to compensate volume loss, N_2 was injected at the time of sampling. For ICP samples, about 1.5 mL of sample was taken at each timestep and filtered through 0.22 μm nylon syringe filters prior to immediate fixing in 2 % HNO_3. An extra sample (0.5 mL) was taken when pH was measured.

At the end of 24 h of reaction, each bottle was sacrificed to collect any solids precipitated. Solids were centrifuged and triple rinsed with N_2-purged water as quickly as possible to try and prevent oxidation. Fe (II) experiments always changed color during rinsing from the original off-white in the bottles to shades of brown or dark greenish brown. Immediately after the final centrifuge step, the solid samples were frozen at −20 °C to minimize any further oxidation. Frozen samples were freeze-dried for further analyses and long-term storage. Often the Fe(II) samples would be tinged orange after freeze-drying, indicating some oxidation during the drying process.

2.2. Analytical methods

Concentrations of total metal (free + bound) were measured by inductively coupled plasma optical emission spectroscopy (ICP-OES) using a Thermo iCAP 7400 DUO ICP-OES (1 ppm Sc internal standard). Samples fixed in nitric acid were diluted with 2 % HNO_3 to be in range of the standards. Analytical error including variability introduced during dilution of samples (1σ standard error) was 7 μM for Fe, 19 μM for Co, and 11 μM for Ni based on check standards throughout each ICP run session over 4 months. The pH was measured at room temperature using a semi-micro single junction pH electrode filled with 3.5 M KCl and AgCl. UV–Vis spectra were collected on an Evolution 60 spectrophotometer, scanning from 300 to 900 nm at a resolution of 1 nm. Complexed metal solutions were loaded in plastic cuvettes with working distance of 1 cm and blank-subtracted using DI water as the blank.

2.3. Characterization of solid products

To observe mineral product morphologies, mineral products were mounted on carbon tape and coated with ~10 nm of gold before imaging with a Tescan Mira3 FEG-SEM (scanning electron microscope) equipped with an energy dispersive X-ray (EDAX) detector at the Physics Department of Washington University in St. Louis. For secondary electron (SE) imaging, the accelerating voltage was 15 keV at a working distance of 15 mm. In addition, the elemental composition of different crystal morphologies was confirmed with EDS (20 keV at a working distance of 17 mm).

Raman spectroscopy was attempted, however the laser intensity had to be set very low for Co and Fe-bearing solids not to be affected by the laser. Because of this limitation, the signal to noise ratio was extremely low. Hence, Fourier Transform Infrared Spectroscopy (FTIR) spectroscopy was utilized instead to characterize the amorphous solids produced. Mid-IR attenuated total reflectance (ATR) spectra were obtained on powders using a Nicolet iS10 FTIR (Thermo) equipped with a KBr beamsplitter and a diamond ATR accessory. Twenty scans were averaged at a resolution of 0.48 cm^{-1} for each sample. The spectrometer was continuously purged with liquid N_2 to remove H_2O vapor and CO_2 in the system and to cool the detector reducing the thermal noise.

For samples with larger crystal sizes (>10 μm), X-ray diffraction was used to confirm the mineral identifications identified by FTIR. Powder XRD analysis was performed on a Bruker d8 Advance diffractometer configured with a Cu source operating at 40 kV and 40 mA and a positive sensitive, energy-dispersive LynxEye XE detector. Hand crushed powder was mounted on a zero-background silicon sample holder (MTI). XRD scans were performed using a 0.02° step size, 0.5 s count time per step at 15 rotations per minute of the sample holder. Initial processing of raw data and mineral identification based on pattern matching used the Diffrac.Eva program (Bruker), with final Rietveld refinement performed in the TOPAS software (Bruker).

2.4. Precipitation kinetics

To allow a simplified consideration of rates with respect to only the metal concentrations, carbonate solid formation experiments were conducted under metal-limiting conditions with bicarbonate ions greatly in excess of metal concentrations. The rate of metal ions lost due to solid carbonate formation after the initial 'instantaneous' precipitation (within the first 3 min after carbonate addition) follows a 2nd order exponential curve until a steady-state concentration is achieved within 5 h. The apparent rate constant in the absence of Tris (i.e., control) was calculated as the slope of the linear regression of $1/[Me]_{total}$ with time, where [Me] represents the measured concentration of either Co, Ni, or Fe. To isolate the effect of Tris on the rate of solid carbonate precipitation, the expected loss of free metal ions based on the control was subtracted from each time step, as follows:

$$\left([Me] / [Me]_0 - [Me]^C / [Me]_0^C\right) \times [Me]_0$$

Where [Me] or $[Me]^C$ is the concentration of total metal at each time step for the Tris or control experiment, respectively, and the initial concentration expected at time zero, $[Me]_0$ or $[Me]_0^C$, is kept the same for each. The fraction of total metal (free + bound) remaining in solution was calculated at each time step to normalize slight variations in the initial concentration between each experiment. To determine the excess fraction in solution, the fraction remaining at each time step in the control was subtracted from the fraction remaining at the corresponding time step of each Tris experiment. This excess fraction was then converted back to excess total metal concentration remaining in solution using the initial metal concentration measured in each experiment. The excess metal is assumed to be complexed with Tris and the subsequent 2nd order apparent rate constant is calculated in the same fashion as the control.

2.5. Saturation index calculations

Calculations of the mineral saturation index ($\log_{10}Q/K_{sp}$) at the conditions of various experiments were performed using Geochemist's Workbench (Bethke, 2022) and the LLNL database (thermo.com.V8.R6+) that was modified to include gaspéite ($NiCO_3$), hellyerite ($NiCO_3{\cdot}6H_2O$), rosasite ($Co_2CO_3(OH)_2$), and chukanovite ($Fe_2CO_3(OH)_2$). Q is the reaction quotient and K_{sp} is the solubility product, equilibrium constant. Thermodynamic log K_{sp} values at 25 °C were used as reported and referenced in Table 2 and adjusted for temperature using the Van't Hoff equation with the following values for ΔH^0 in J/mol: −713.4 for gaspéite (Wallner et al., 2002), −2456.7 for hellyerite (Wallner et al., 2002), and −1798 for both rosasite and chukanovite (Gogol et al., 2024) in the absence of values for each mineral.

3. Results

3.1. The nature of the tris-metal complex

UV–Vis spectra were collected on various metal-Tris mixtures at 25 °C at different pH ranging from 4.6 to 8.4. Absorbance is reported in molar absorptivity to normalize for differences in concentration of metal in each mixture. There is no difference in spectra between the solution of $NiCl_2$(aq) and the Ni-Tris HCl complex, although the bands for the Tris base complex shift in wavelength and intensity as a function of the Tris:Me ratio (Fig. 1a). The dominant band for Ni complexes in the UV range has maxima around 390 nm, with the Tris-base complex slightly blue shifted to 389 and 384 nm (for 1:1 and 3:1 Tris:Ni ratios; pH 7.9 and 8.4, respectively) from both the $NiCl_2$(aq) complex (394 nm; pH 7.3) and Ni-Tris-HCl complex (394 nm; pH 4.6–4.7) (Fig. 1a). The weaker secondary absorption bands in the visible range between 600 and 800 nm are identical in both the $NiCl_2$(aq) and Tris-HCl complex, with the band at 725 nm more dominant than the band at 661 nm (Fig. 1a). The opposite is observed in the Tris-base complex, with the lower wavelength band dominant and blue shifted to 651 and 631 nm for 1:1 (pH 7.9) and 3:1 Tris:Ni (pH 8.4), respectively, and the higher wavelength band (at 729 nm) nonexistent in the 3:1 complex (Fig. 1a).

Only one pair of absorption bands are present in the visible range between 400 and 600 nm for Co complexes at lower pH (Fig. 1b). As with Ni, the bands are identical in both the $CoCl_2$(aq) and Tris-HCl complex, with the band at 512 nm more dominant than the band at 480 nm, despite slight differences in pH (6.9 for Co++, 5.1 for the 1:1 Tris:Co ratio and 5.6 for the 3:1 ratio), consistent with the observations of Dotson (1972). This relative band height remains the same in the Tris-buffer (Tris-HCl and Tris base mix) complexes, unlike the Ni complexes, but the bands are blue shifted to 476 nm for the dominant band and 447 nm for the weaker band at both the 1:1 ratio (pH 8.1) and the 3:1 ratio (pH 8.3) (Fig. 1b). Also unlike the Ni complexes, Co complexed to the Tris buffer mixture produced an additional peak in the UV range (<250 nm) with a much higher extinction coefficient (~75 $LM^{-1}cm^{-1}$), possibly indicative of metal to ligand charge transfer with subsequent metal oxidation (e.g., autoxidation to Co^{+3}), producing a more stable low spin 3 d^6 complex (Leite et al., 2000). When 100 % Tris base was used to create the complex, the pH was 8.6 for the 1:1 ratio and 9.1 for the 3:1 ratio and a brown precipitate formed immediately on contact with air in both solutions, preventing analysis. The buffer complex used in the carbonate experiments, however, is stable in air and is shown in Fig. 1b.

Stable solutions of Fe(II) complexes with Tris-HCl are colorless and have no peaks in the visible range (pH 4.8; Fig. 1c and d). Attempts to produce the Fe-Tris base complex and the Fe-Tris buffer complex resulted in the precipitation even in the anoxic gas-tight bottles (likely chloride green rust), possibly similar to the brown precipitate that formed with Co-Tris base mixtures. However, the effect of Fe on the mixed metal complexes with Tris-HCl is noticeable, causing blue shifts in the bands and decreased intensity for both Fe–Ni and Fe–Co mixtures (Fig. 1c and d, respectively), although the pH is similar to the single Ni or Co complexes (pH 5.3 for Fe + Ni and pH 4.9 for Fe + Co). The implications of these shifts with pH are discussed further in section 4.2.

3.2. Effect of tris on metal carbonate solubility at 25 °C and 80 °C

To determine the efficiency and selectivity of Tris-HCl at complexing Fe, Ni, and Co under carbonate saturated conditions, batch experiments were conducted at 25 °C and 80 °C with a range of ligand:metal ratios (0.25, 0.5, 1, 2, and 3). Initial concentrations in each experiment were nominally 5 mM of metal ($FeCl_2$, $CoCl_2$, or $NiCl_2$) complexed to variable amounts of Tris-HCl (ligand:metal solutions range in pH from 4.5 to 5.5), 100 mM of $NaHCO_3$, 5 mM of Na_2CO_3 to buffer the final pH at ~ 8. The decrease in metal concentration over time was monitored and pH was measured in the initial and/or final samples (Supplemental Data Table). After an initial near-instantaneous loss (prior to the first sample taken within 3 min of carbonate addition), the rate of decline in concentration for all metals slows over the first 3–4 h (Fig. 2) and reaches a steady-state concentration that persists for over 24 h (Supplemental Data Table). The initial loss is much greater and steady-state concentrations much lower for each corresponding condition at 80 °C

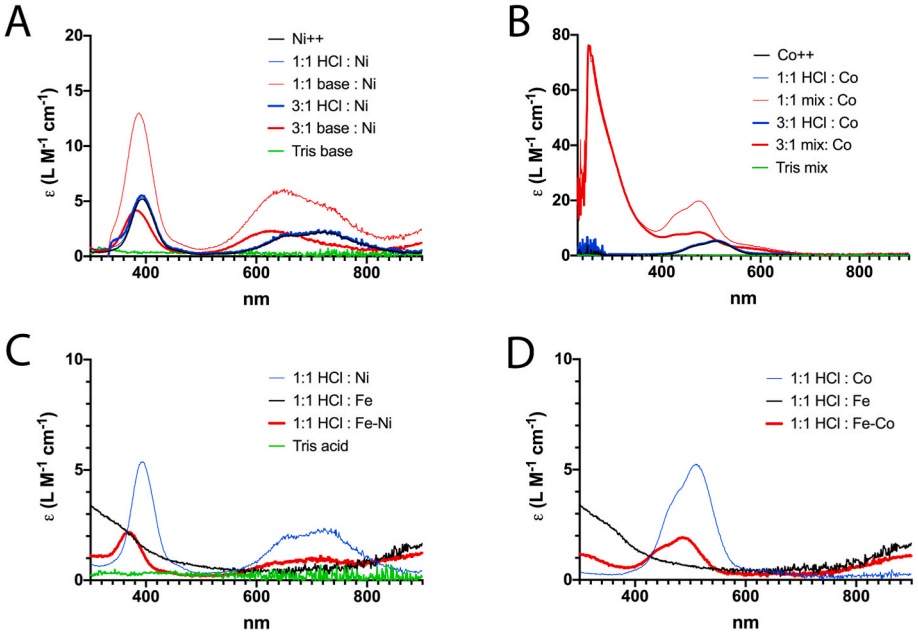

Fig. 1. UV–Vis spectra of Tris-metal complexes compared to solutions of metal chloride salts (designated as Me++). Comparison of Me++ solutions with Tris HCl:Me or Tris base:Me or Tris buffer:Me (designated as mix) solutions at 1:1 or 3:1 ratios for (A) Ni and (B) Co. Comparison of the 1:1 Tris HCl:Me complex for Fe, Ni, and Fe–Ni mixture (C) and Fe, Co, and Fe–Co mixture (D), where ε was calculated using the total metal concentration. Spectra for Tris base, Tris buffer (labeled mix), and Tris acid with no metal in solution are shown in green in panels A, B, and C, respectively. (For interpretation of the references to color in this figure legend, the reader is referred to the Web version of this article.)

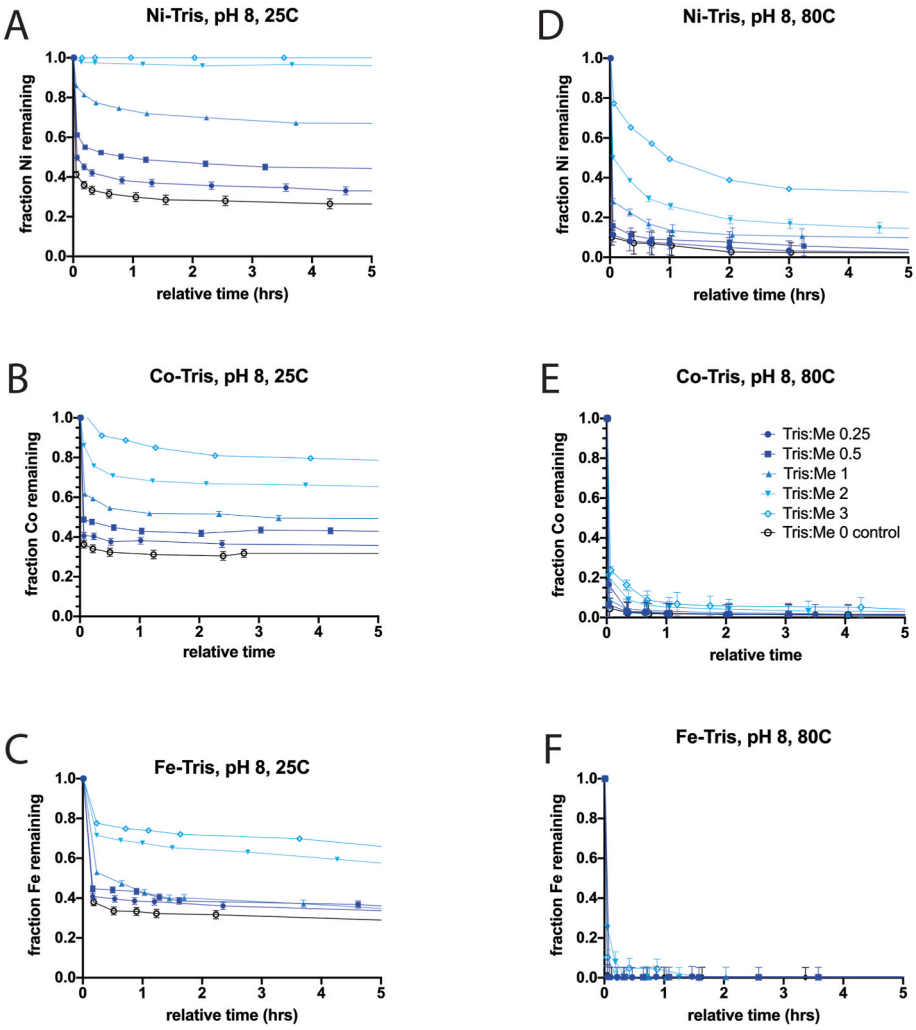

Fig. 2. Time series as the fraction of metal lost due to precipitation at 25 °C for Ni, Co, Fe (A-C, respectively), and at 80 °C for Ni, Co, Fe (D-F, respectively). All experiments are for Tris-HCl (pH 4.5–5.5 prior to CO_3^{2-} addition) complexed with metal. Error bars represent ±20 μM precision (1σ) in the analysis.

(Fig. 2d–f). Both the instantaneous fraction of metal lost and the steady state concentration after 5 h is inversely proportional to the Tris:metal ratio for Ni, Co and Fe (Supplemental Data Table and Fig. 2). In addition, the rate of precipitation of carbonate decreases with increasing Tris: metal ratio, allowing an evaluation of the mechanism of ligand exchange reaction between Tris and carbonate ions (Fig. 2).

3.3. Effect of pH on metal carbonate solubility at 25 °C

The ability of Tris buffer (pH 6.5–7.5) to bind nickel and cobalt was evaluated at the same experimental conditions with Tris-HCl (pH 4.5–5.5) in the presence of aqueous carbonate buffered at pH 8 (Fig. 3a and b compared to Fig. 2a and b). When the complex is formed at higher pH, the amount of solid carbonate precipitated was greater, with a much greater impact on Co than Ni. The impact of pH on the strength of the metal-Tris complex in alkaline carbonate-rich solutions was also evaluated at 25 °C using initial concentrations of 3 mM metal and 9 mM Tris-HCl. The final pH was varied by adjusting the ratio of HCO_3^- to CO_3^{2-} (total carbonate maintained at 100 mM) to buffer the pH during the experiment. The decrease in metal concentration over time was monitored and pH was measured in the initial and/or final samples (Supplemental Data Table). The strength of the Ni-Tris complex is unaffected by pH at a Tris:Ni ratio of 3, with complete inhibition of carbonate precipitation even at pH 10.5 (Fig. 3c). However, the ability of Tris-HCl to bind cobalt and iron is less at higher pH, with almost no inhibition of precipitation at pH > 10 (Fig. 3c). The implications of these observations are discussed further below.

3.4. Effect of metal mixtures on metal carbonate solubility

The impact of mixed metal-Tris complexes on carbonate precipitation was evaluated with simple mixtures of 1 mM Co or Ni with 2 mM Fe compared to single-metal control experiments at the same concentrations. The Tris-total metal ratio was set to 3, 1, or 0 with 100 mM of $NaHCO_3$, 5 mM of Na_2CO_3 to buffer ~ pH 8 in all experiments. The decrease in metal concentration over time was monitored and pH was measured in the initial and/or final samples (Supplemental Data Table). The lower concentrations of metal (1 mM rather than 5 mM) in the single metal control experiments show a more distinct difference in metal carbonate solubility, with Ni > Co > Fe at 25 °C and 80 °C (Fig. 4). The addition of Tris decreased the amount of carbonate precipitation as a function of the Tris:metal ratio in all single-metal control experiments at 25 °C and 80 °C, as expected based on the previous experiments (Fig. 4). The presence of Fe noticeably increased the amount of Ni and Co precipitation in the absence of Tris at both 25 °C and 80 °C, without affecting the amount of Fe precipitation. At 25 °C with a Tris:metal ratio of 1, the addition of Fe caused a marked increase in Ni or Co carbonate precipitation (Fig. 4b and c) at the apparent expense (decrease) of Fe precipitation (Fig. 4a). With a higher Tris:metal ratio of 3, the effect of Fe is negligible on Ni and Co, but the presence of Ni or Co decreases the

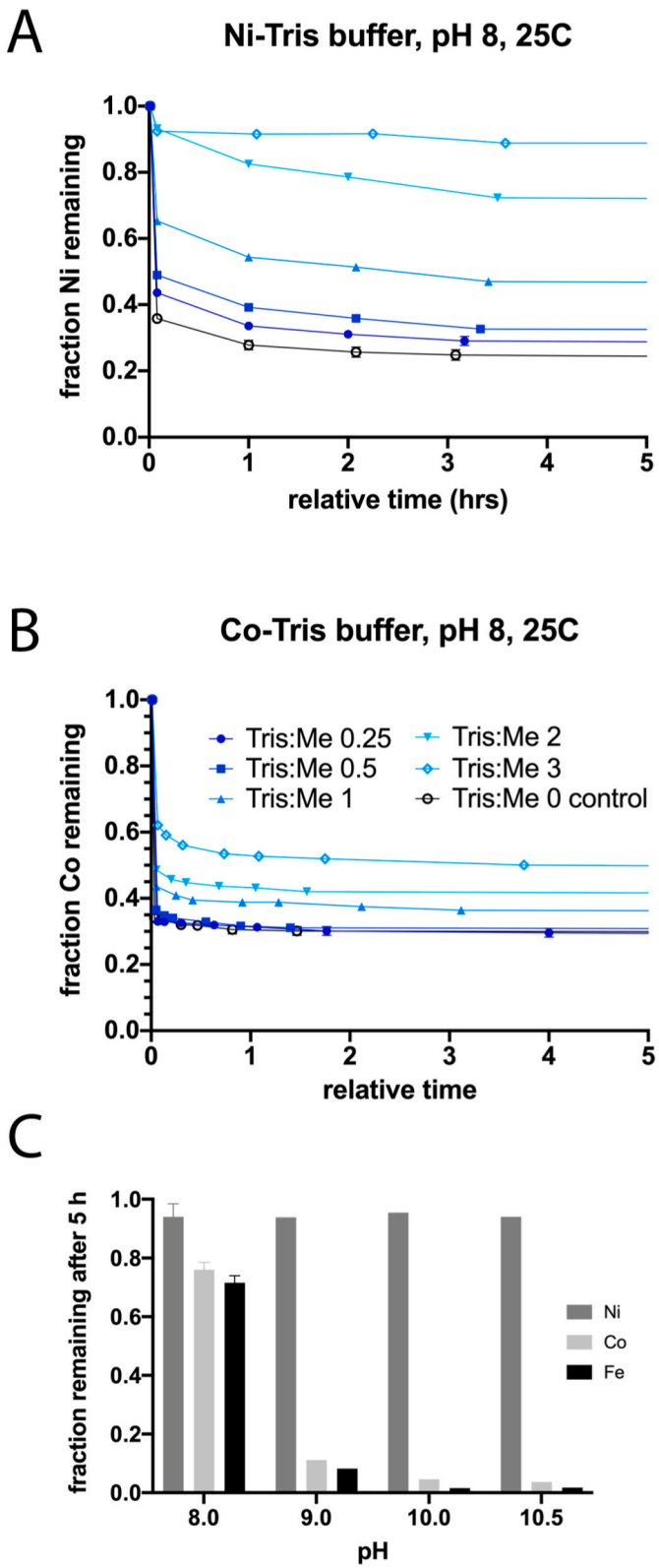

Fig. 3. Time series of the fraction of metal lost using Tris buffer (pH 6.5–7.5 prior to CO_3^{2-} addition) at variable Tris:metal ratios for Ni (A) and Co (B). Error bars are smaller than the size of the symbols, reflecting ±20 μM precision in the analysis. (C) Fraction of metal remaining in solution at 25 °C after 5 h using a Tris-HCl:metal ratio of 3 for Fe (black), Ni (dark grey), and Co (light grey) at variable pH set by the carbonate-bicarbonate buffer. Error bars for pH 8 experiments are based on 3 replicate experiments.

amount of Fe carbonate precipitated by 1.5–2 times relative to the single-metal Fe control (Fig. 4a). At 80 °C, the rate of carbonate precipitation in all experiments results in very low concentrations remaining in solution after 5 h (Fig. 4, right scale). However, a similar pattern exists where the addition of Fe increases the amount of Ni and Co carbonate precipitation at Tris:metal ratios of 1 and 3 (Fig. 4b and c), while the presence of Ni and Co does not affect Fe precipitation (Fig. 4a).

3.5. SEM and XRD characterization of minerals produced

Precipitates formed from single metal-carbonate solutions at 25 °C were amorphous or on the nanometer scale (Fig. 5a–c). At 80 °C, Ni remained as an amorphous solid regardless of the addition of Tris, although Co and Fe produced more crystalline shapes on the order of 5–10 μm in size (Fig. 5d–i). The relative abundance of subhedral to euhedral crystals increased with the addition of Tris at the expense of the amorphous/plate-like solid for both Co and Fe (compare Fig. 5e–h and f-i). In the single metal experiments, only Co and Fe at 80 °C produced precipitates ordered enough to identify using XRD. The XRD spectrum of the Co control at 80 °C (Fig. 5e–S1) fit rosasite ($Co_2CO_3(OH)_2$), while the addition of Tris (Fig. 5h) produced a mixture of 87 % sphaerocobaltite and 13 % rosasite (Fig. S1), consistent with the two distinct morphologies seen in SEM. The Fe control at 80 °C (Fig. 5f–S2) matched a combination of siderite (46 % $Fe^{2+}CO_3$) and chukanovite (51 % $Fe_2CO_3(OH)_2$). With increasing Tris (Fig. 5i), XRD confirms siderite abundance increases to 90 % with 10 % chukanovite remaining (Fig. S2), consistent with the SEM observations.

Precipitates formed during mixed metal experiments at 25 °C primarily show the same nanocrystalline morphologies seen in the equivalent single metal experiments (Fig. 6a and b). The Fe–Ni mixture produced the occasional rosette of plates in a matrix of nanocrystalline platelets, however, EDS spot analysis of the two morphologies (Fig. 6a, spots 1 and 2) indicates the same Fe:Ni ratio (2.1 Fe:Ni by at%; Figs. S5 and S6). The Fe–Co mixture at 25 °C produced uniform small clusters of acicular nanocrystalline needles (Fig. 6b) with a similar Fe:Co ratio based on EDS analysis (2.4 Fe:Co by at%; Fig. S7). Unlike the single metal Co experiments at 80 °C, mineral morphology in the Fe–Co mixture did not change as a function of Tris abundance but retained the same nanocrystalline habit seen at 25 °C (Fig. 6c) and a similar Fe:Co ratio as at 25 °C (2.3 Fe:Co by at%; Fig. S8) based on EDS analysis. Also unlike the single metal Ni experiments at 80 °C, the mineral morphology in the Fe–Ni mixtures did change with increasing Tris abundance (Fig. 6d). At a Tris:Ni ratio of 1, two new morphologies developed at the expense of the nanocrystalline matrix with Ni partitioning differently in each, based on EDS: larger plates (spot 3: 2.8 Fe:Ni by at%; Fig. S9), fat rods (spot 4: 5.9 Fe:Ni by at%; Fig. S10), with residual nanocrystalline matrix (spot 5: 1.8 Fe:Ni by at%; Fig. S11). At a Tris:Ni ratio of 3, larger plates and spherical clusters of tiny hexagonal crystals form at the expense of the nanocrystalline matrix, again with Ni partitioning differently in each, based on EDS: larger plates (spot 6: 1.0 Fe:Ni by at%; Fig. S12), spheres (spot 7: 6.2 Fe:Ni by at%; Fig. S13), with residual nanocrystalline matrix (spot 8: 0.8 Fe:Ni by at%; Fig. S14).

3.6. FTIR characterization of minerals produced

FTIR spectra of precipitates made from single metal solutions at 25 °C are identical regardless of the ligand–metal ratio. Carbonates were produced with all 3 metals (Fig. 7a), although the broad peak around 3300 cm^{-1} and the shoulder at ~1650 cm^{-1} indicate H_2O bound within the structure (White, 1974). The ν_2, ν_3, and ν_4 CO_3 peaks are shifted lower (Table 1) relative to the corresponding pure carbonate phases of gaspéite ($NiCO_3$), cobaltite ($CoCO_3$), and siderite ($FeCO_3$), which should occur at 866–876 cm^{-1}, 1420–1485 cm^{-1}, and 737–751 cm^{-1}, respectively (White, 1974; Huang and Kerr, 1960; Weir and Lippincott, 1961; Kohls and Rodda, 1966). This is likely due to the effect of hydrogen bonding in the hydrated phases that shifts the CO_3 peaks lower (Bette

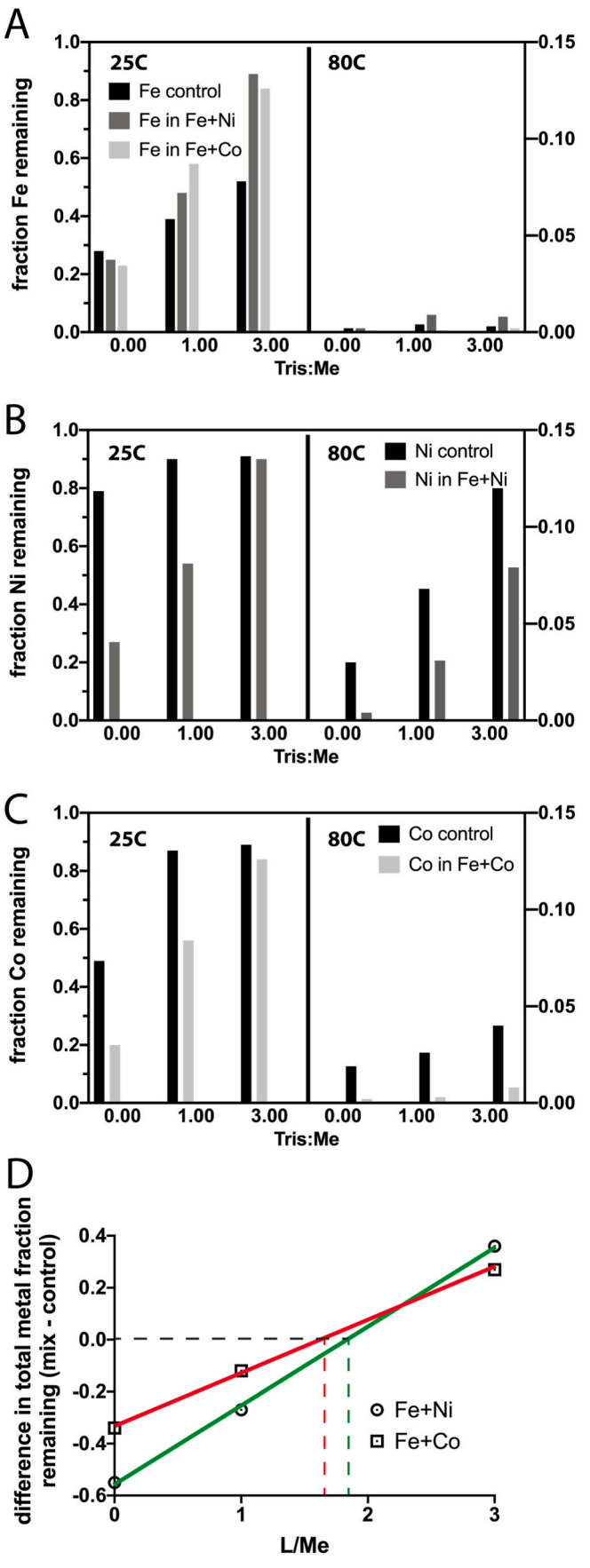

(caption on next column)

Fig. 4. Change in the fraction of total metal remaining in solution after 5 h of reaction at pH 8, 25 °C (left scale) and 80 °C (right scale; note the difference). Comparison with controls of single metals at 1 mM or 2 mM initial concentration are shown for Fe (A), Ni (B), and Co (C) at Tris-HCl:metal ratios of 0, 1 and 3. (D) Comparison of differences between metal mixture and single metal results at 25 °C from A-C for Fe + Ni (green) and Fe + Co (red). The dashed lines indicate the Tris:Me ratio at which the carbonate precipitation in the mixed metal experiments would be equivalent to the single metal control. (For interpretation of the references to color in this figure legend, the reader is referred to the Web version of this article.)

et al., 2016). Likewise, the weak band at 1090 (ν_1 CO_3) becomes IR active when symmetry of the CO_3 anion is reduced (Frost et al., 2007). In addition, the Fe carbonate FTIR spectra produced at 25 °C has a double peak at the ν_2 frequency (818 and 858 cm^{-1}) and a distinct shoulder on the ν_3 peak (at 1530 cm^{-1}), suggesting the beginning of field splitting caused by crystallographically different carbonate ions in the structure (Frost et al., 2007; Stoilova et al., 2002). The peak at 546 cm^{-1} corresponds to a metal-O stretching band.

The ligand–metal ratio does affect the FTIR spectra of precipitates formed from single metal solutions at 80 °C and significant differences in crystal structure appear between the three transition metals (Fig. 7b). The Fe control (no Tris) at 80 °C looks different than the precipitate formed at 25 °C, with a splitting of ν_2 and ν_3 into two peaks (at 811 and 858 cm^{-1} and 1380 and 1560 cm^{-1}, respectively; Table 1). There is notably a very minimal band for H_2O centered around 3300 cm^{-1}, but instead a weak peak at 3490 cm^{-1}, possibly reflecting an O–H stretching band. The metal-O stretching band at 541 cm^{-1} is also still present and this spectrum matches well with that of chukanovite (Rémazeilles and Refait, 2009; Azoulay et al., 2012). However, the addition of Tris during precipitation alters the structure, removing the O–H, H_2O and metal-O bands and simplifying the ν_2 and ν_3 CO_3 bands to single peaks at 856 and 1380 cm^{-1}, respectively (Table 1). The ν_3 band has a noticeable tail between 1000 and 1380 cm^{-1}, but the imbedded peaks were not

resolved. The Ni control (no Tris) at 80 °C also looks similar to the control at 25 °C with minor differences in stronger bands that are slightly shifted in ν_4 CO_3 (from 707 to 620 cm^{-1}) and in ν_1 CO_3 (from 1090 to 1050 cm^{-1}) and a weaker band in the ν_3 CO_3 region. The addition of a peak at 988 cm^{-1} was assigned to the δ-OH bending region (Table 1). With the addition of Tris during precipitation, the structure becomes closer to that formed at 25 °C except with closely spaced double peaks in the ν_1, ν_3, and ν_4 CO_3 regions (Table 1). The Ni carbonates formed at 80 °C are both hydrated, with a pronounced broad band centered at 3300 cm^{-1}. The Co control (no Tris) at 80 °C is quite different from the control at 25 °C and matches well with spectra of minerals in the rosasite family (Frost et al., 2007; Rémazeilles and Refait, 2009; Azoulay et al., 2012). The addition of O–H stretching bands at 3380 and 3500 cm^{-1}, the splitting of the ν_3 CO_3 band into clearly distinct peaks (at 1350 and 1540 cm^{-1}) and the splitting of the ν_4 CO_3 band into 4 peaks (Table 1) are all features of the rosasite crystal structure: $Me_2CO_3(OH)_2$ (where Me can be any transition metal). As with Ni and Fe, addition of Tris during precipitation causes the precipitate to become more like pure Co carbonate (Fig. 7b), with a decrease in peak heights in the O–H stretching region and the ν_2 and ν_4 CO_3 regions (<900 cm^{-1}) as well as a decrease in the 1540 cm^{-1} peak, suggesting less field splitting of the CO_3 anions in the structure. Overall, the FTIR of the 80 °C experimental products suggests that addition of Tris during precipitation for all three transition metals allows more pure carbonates to form, consistent with the SEM observations seen in Fig. 5 and XRD results.

Both the Fe–Ni and Fe–Co mixed metal experiments at 25 °C produced solids with features from both endmember controls, particularly in the ν_3 and ν_4 CO_3 regions (Fig. 7c and d). The ν_3 region in the Fe–Ni mixtures is weakened and peaks are shifted relative to both endmembers, yet in the Fe–Co mixtures this region maintains the structure of the Fe endmember (Table 1). The Me–O stretching band in both mixtures is

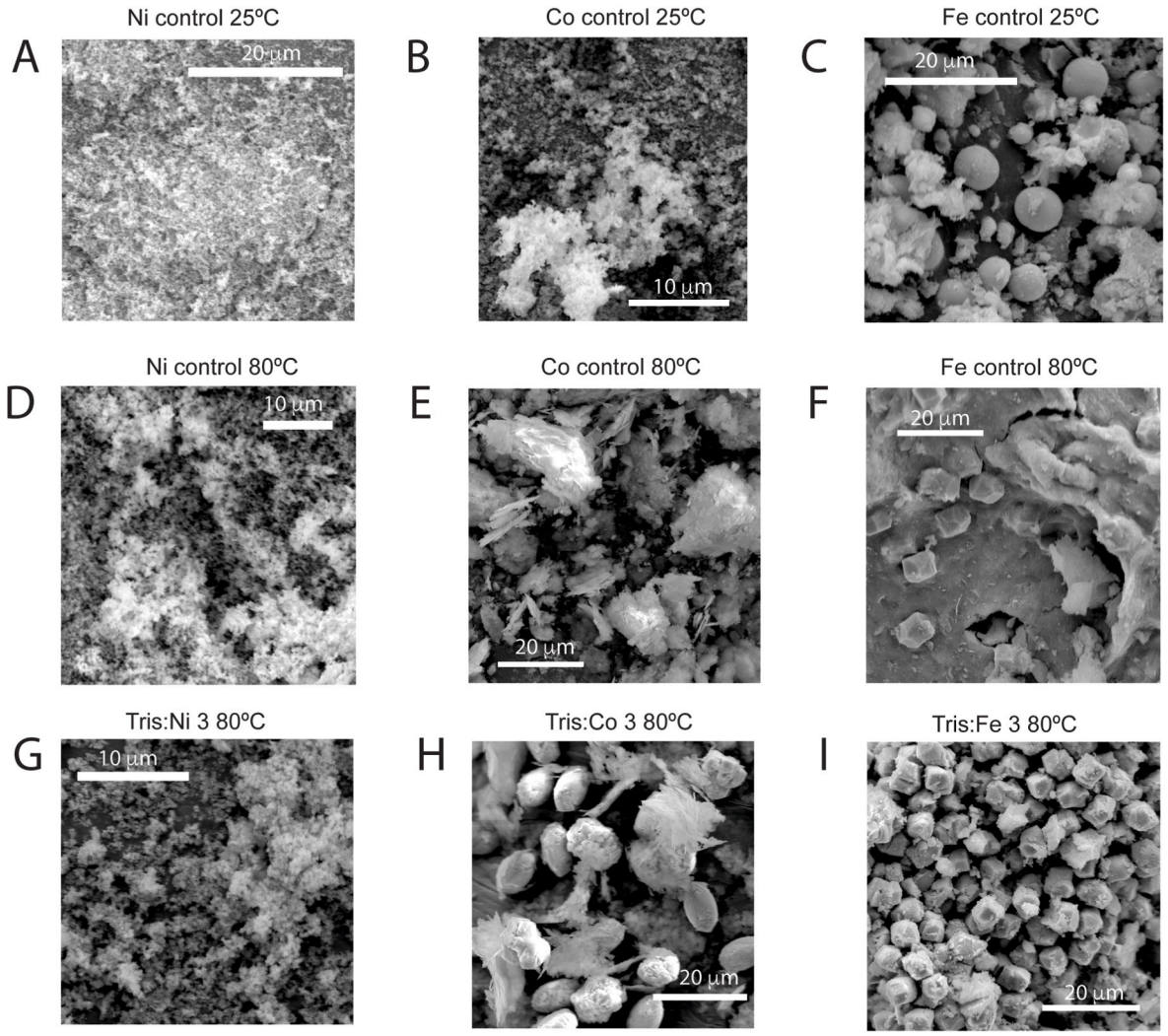

Fig. 5. SEM SE images of precipitates from single metal experiments formed at 25 °C (A–C) and 80 °C (D–I); Precipitates formed at 80 °C in the absence of Tris (D–F) and presence of Tris at the 3:1 ratio with respect to metal (G–I) for Ni (D and G), Co (E and H), and Fe (F and I).

present, however in the Fe–Ni mixtures the ν_4 band is less intense than the Me–O stretching band, while the reverse occurs in the Fe–Co mixture. In both mixtures, the higher Tris abundance does not significantly change the spectra. Overall, the Fe–Ni mixture has stronger features of hydrous carbonate than the Fe–Co mixture, which is more like a hydrous rosasite-type mineral. A similar pattern occurs in mixtures at 80 °C but with more pronounced features, particularly in the ν_1 band that would indicate greater asymmetry in the CO_3 anion within the lattice (Fig. 7e and f). With increased Tris in the Fe–Ni mixtures, the spectra shifts from a rosasite-like phase to a hydrated carbonate more similar to the Ni only control (Fig. 7e; Table 1). Increasing Tris in the Fe–Co mixtures did not produce significant changes in the spectra, which retain much of the features of the Fe only control that indicates chukanovite (Fig. 7f; Table 1).

4. Discussion

4.1. Carbonates produced in the absence of tris

The carbonates produced at 25 °C without Tris were all amorphous or nanocrystalline (Fig. 5a–c) hydrated carbonates based on FTIR spectra (Fig. 7a). The low temperature hydrated form of nickel carbonate is known as hellyerite ($NiCO_3{\cdot}6H_2O$) and the solubility product has been determined ($\log K_{sp} = 10.64$; Wallner et al., 2002). Amorphous hydrated cobalt carbonate with matching FTIR characteristics has been reported (Katsikopoulos et al., 2008) but the K_{sp} for this phase was not determined. The amorphous hydrated form of iron carbonate (known in the literature as AFC) has been characterized as $Fe_2CO_3(OH)_2$ by Jiang and Tosca (2019) but the K_{sp} has not been determined (Dideriksen et al., 2015). The anhydrous form of chukanovite ($Fe_2CO_3(OH)_2$) was reported in Kim et al. (2017) to have a $\log K_{sp}$ of 16.2 (reaction 23, Table 2). The $\log K_{sp}$ of crystalline $CoCO_3$ is 9.98 (Riechers et al., 2022, based on data from Smith et al., 1976; Naumov et al., 1974) and is 10.24 for siderite ($FeCO_3$) (Singer and Stumm, 1970) (Table 2), suggesting the relative stability of Co is greater than Fe. However, we are not making thermodynamically stable crystalline minerals at 25 °C, and our observed relative supersaturation trend is Fe > Co > Ni. The FTIR spectrum for amorphous Fe carbonate in the control experiment at 25 °C has some characteristics of chukanovite ($Fe_2CO_3(OH)_2$, such as the double peak at the ν_2 frequency (818 and 858 cm^{-1}) and a distinct shoulder on the ν_3 peak (at 1530 cm^{-1}), but no peaks in the O–H stretching region that are present in crystalline chukanovite (Rémazeilles and Refait, 2009; Azoulay et al., 2012) and instead exhibits the broad H_2O band centered at 3220 cm^{-1}. The deviation in our observed saturation order relative to crystalline minerals may be explained by the difference in mineralogy of the Fe carbonate precipitate, being a mixed hydroxycarbonate. The saturation index calculated by speciating the fluid in our experiments supports our observation that chukanovite (reaction 23, Table 2) should

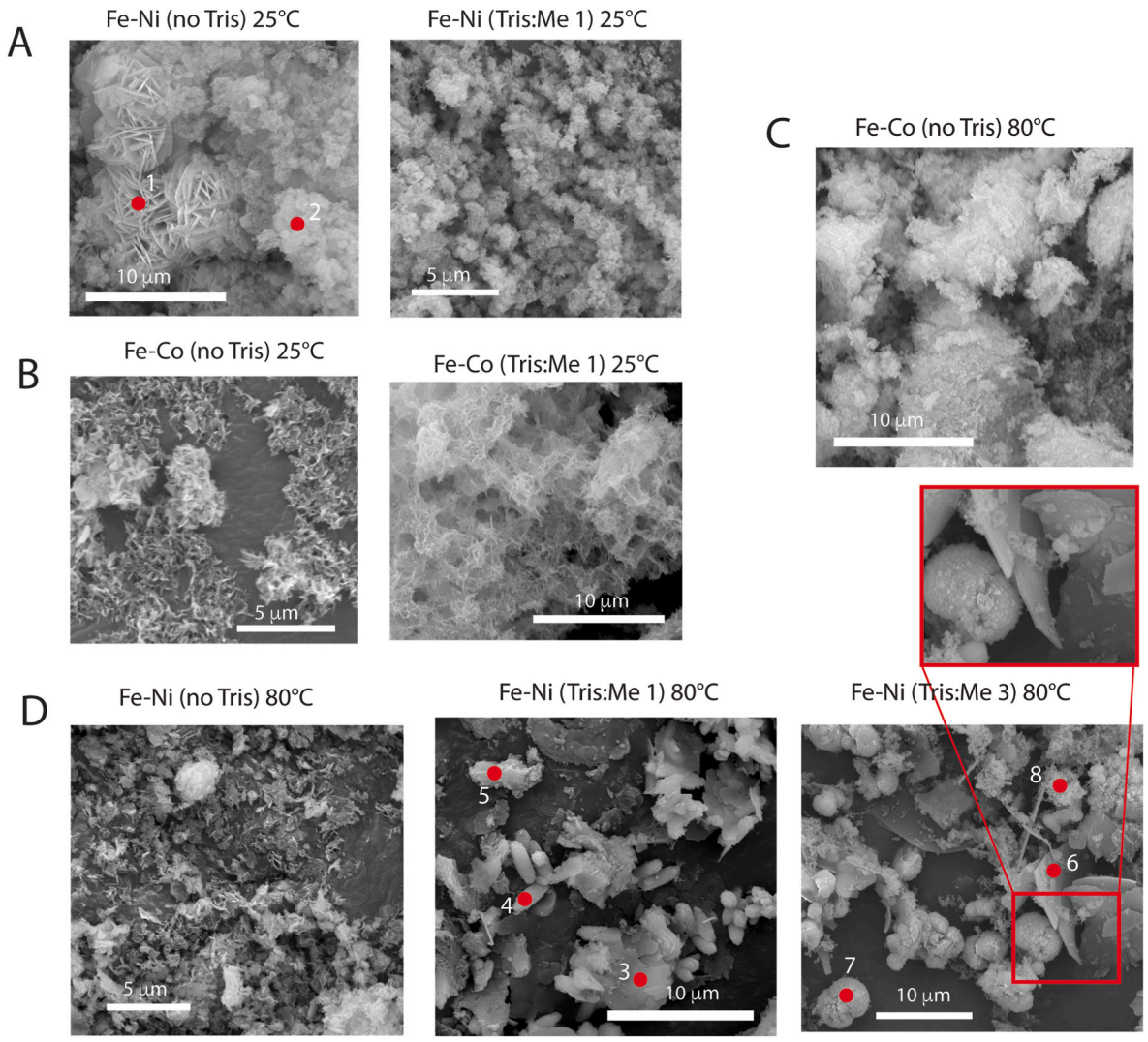

Fig. 6. SEM SE images of precipitates formed in mixed Fe–Ni experiment at 25 °C (A) and mixed Fe–Co at 25 °C (B), mixed Fe–Co at 80 °C (C), and mixed Fe–Ni at 80 °C (D). Inset of (D) is enlarged to show the spheres are aggregates of tiny hexagonal platelet crystals. Red dots indicate where EDS spot analyses were taken from different textures; numbers referenced in main text. (For interpretation of the references to color in this figure legend, the reader is referred to the Web version of this article.)

be 10 times more supersaturated than either sphaerocobaltite (reaction 20, Table 2) or hellyerite (reaction 19, Table 2) at pH 8, 25 °C and 5 mM metal (saturation indices of 30.2, 3.2, and 3.5 for Fe, Co an Ni, respectively).

The carbonates produced at 80 °C have different mineral compositions and degrees of crystallinity between the different metals. Although the rate of precipitation increases at higher temperature for Ni, the precipitate formed remains essentially the same nanocrystalline hydrous carbonate, as seen in SEM and FTIR (Figs. 5d and 7b). In contrast, the Co phase precipitated at 80 °C is primarily a rosasite-like mineral ($Co_2CO_3(OH)_2$) based on XRD and adopts a platy morphology in SEM (Fig. 5e), consistent with the monoclinic crystal structure of minerals in the rosasite family (Frost et al., 2007). Our FTIR spectrum in the absence of Tris (Fig. 7b) matches well with that reported for a synthetic standard of $CoCO_3{\cdot}Co(OH)_2{\cdot}H_2O$ by Katsikopoulos et al. (2008), and reportedly has a much higher $logK_{sp}$ than for Co carbonate (30.3, Table 2; González-López et al., 2018). The Fe precipitate formed at 80 °C was a mixture of amorphous material and rhombohedral crystals based on SEM (Fig. 5f), and XRD confirmed both siderite (46 %) and chukanovite (51 % $Fe_2CO_3(OH)_2$) (Fig. S2). The rhombohedral crystals are consistent with the trigonal rhombohedral crystal structure of siderite (Effenberger et al., 1981). The FTIR spectrum in the absence of Tris also contains some characteristics of chukanovite, with a stronger band at 1560 cm^{-1} and the addition of a tiny band at 3490 cm^{-1} (Fig. 7b). The solubility products for the minerals produced at 80 °C predict a supersaturation order of Co (rosasite) ≫ Fe (chukanovite) > $NiCO_3$ (hellyerite) > $FeCO_3$ (siderite) > $CoCO_3$ (Table 2) and are broadly consistent with the calculated saturation indices at 80 °C: 51.29 (rosasite) > 34.92 (chukanovite) > 16.54 (hellyerite) > 14.09 (sphaerocobaltite) > 5.08 (siderite).

4.2. The effect of ligand-metal exchange on rates of carbonate precipitation

The dissociation constant for Tris has been determined (Bates and Hetzer, 1961), with the stability of Tris acid relative to Tris base at pH 8 higher at 25 °C than at 80 °C (Table 2). Considerably more attention has been paid to the Ni(II) complexes of Tris than for the Co(II) and Fe(II) complexes, primarily due to the rapid oxidation and subsequent precipitation of Fe and the relatively recent interest in Co (Hunt et al., 2015; Sarker et al., 2022). For the Ni(II) Tris complexes, the monomer (NiL^{+2}; reaction 4, Table 2) is thermodynamically more favorable than the dimer (NiL_2^{+2}; reaction 5, Table 2), although at higher pH, the existing coordinated Tris tends to lose proton(s) and become amino-alcoholate

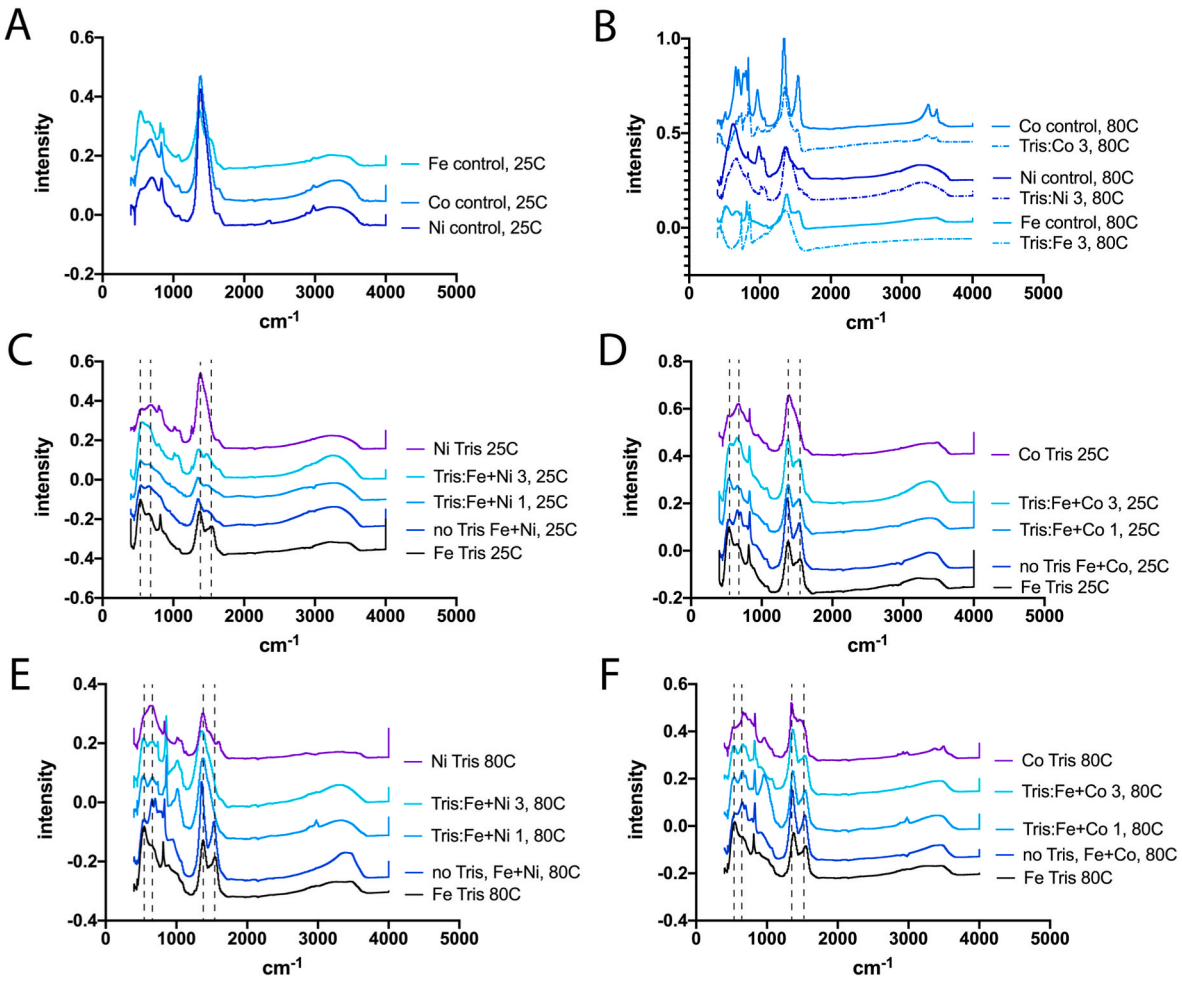

Fig. 7. FTIR spectra of metal carbonates formed at 25 °C (A) and 80 °C (B). Precipitates formed in the Fe–Ni mixtures (C) and the Fe–Co mixtures (D) at 25 °C compared to their respective single-metal experiments. Precipitates formed in the Fe–Ni mixtures (E) and the Fe–Co mixtures (F) at 80 °C compared to their respective single-metal experiments. Spectra are offset in the vertical axis for clarity. Dashed lines mark the bands in the controls for visual comparison with the mixed metal precipitates.

chelates (e.g., $H_{-1}L^{-}$ and $H_{-2}L^{-2}$; Table 2), altering the complex and producing acidity (reactions 6 and 7, Table 2; Bai and Martell, 1969). According to Hall et al. (1962), NiL^{+2} is completely produced at pH 6.9, a 20 % mixture of NiL_2^{+2} with NiL^{+2} is produced at pH 7.5, and from pH 7 to 10 protons are lost from the complex, leading to the complex $Ni_2(H_{-1}L)_3^{+}$. However, the crystalline complex formed from Ni-Tris was determined to be $Ni(H_{-1}L)(L)^{+}$ by Dotson (1972), in which Ni is completely octahedrally coordinated with an amine and alcohol group from 2 Tris molecules. Our UV–Vis spectra at pH 8 (Fig. 1a) are similar to those for the $Ni(H_{-1}L)^{+}$ complex at pH > 8.3 reported in Hall et al. (1962), which is also consistent with the interpretations of Bai and Martell (1969). In contrast, Hall et al. (1962) suggest the $Ni(HL)_2^{+2}$ complex dominates at pH < 7.2.

The crystalline complex formed from Co-Tris mixtures has been shown to be an oxide-coupled dimer of $(Co(H_{-1}L)^{+})_2$, with two nearly independent high-spin Co(II) nuclei each sharing coordination with the O^{-} alcohol (reaction 8, Table 2; Dotson, 1972), although the stability constant was not determined. In this complex, the amine group in each Tris molecule is bonded to the opposite Co ion from its alcohol groups, producing a high spin five-coordinate complex with C3 symmetry and a trigonal bipyramidal structure (Dotson, 1972). Our UV–Vis spectra (Fig. 1b) suggest that as the pH approaches the pK_a of Tris (pH ~ 8.1), the nature of the complex changes more substantially for Co than for Ni, consistent with crystallization experiments conducted by Dotson (1972). These spectra suggest that under more alkaline conditions near the pK_a of Tris (pH ~ 8.1; Bates and Hetzer, 1961), the Δ_0 field splitting of the 3d orbital in both the Ni-Tris and Co-Tris complex increases (Table 3). However, because Ni is a 3 d^8 metal and Co is 3 d^7, the overall stabilization energy (SE) is higher for Ni complexes than Co complexes due to the extra paired electrons in the t_{2g} orbitals (Table 3), making the Ni complexes stronger than the Co complexes. To our knowledge, no studies of Fe(II) complexation with Tris have been reported.

To understand the effect of Tris on the rate of carbonate precipitation for each metal at 25 °C, the excess fraction of metal remaining (i.e., the Tris-bound fraction) was determined by subtracting the corresponding time step of the control experiment (no Tris) in each experiment (see Methods). The change in this residual over time is assumed to be due to the Tris-carbonate ligand exchange that is necessary to allow further precipitation of carbonate mineral at varying Tris:metal ratios. The excess fraction remaining after the first 5 h increases with increasing abundance of Tris-metal complex (Fig. 8a), with the strength of the Tris complex consistently following the order Ni > Co > Fe, regardless of whether Tris-HCl or Tris base was used. This observation suggests the rate of ligand exchange also contributes to the overall rate of carbonate precipitation at 25 °C. The strength of both the Ni and Co complex decreases significantly (~1.5 times for Ni and ~3 times for Co) when the complex forms at higher pH (~7 in Tris buffer vs. ~5 in Tris-HCl) (Fig. 8a), consistent with the pattern in SE of the complexes based on the UV–Vis spectra (Table 3). The amine in Tris-HCl is protonated (NH_3^{+}) compared to Tris base (NH_2) and therefore must be affecting the strength

Table 1
FTIR peak assignments based on White (1974).

	Metal-oxygen stretch	v_4 CO_3	v_2 CO_3	δ OH bend	v_1 CO_3	v_3 CO_3	v_2 H_2O	v_1, v_3 H_2O	O–H stretching bands
Ni control, 25 °C	–	707	837		1090	1380	1650	3260	
Co control, 25 °C	–	696	829		1070	1380	1640	3320	
Fe control, 25 °C	546	645	818		1080	1380	1650	3220	
			858			1530 (shoulder)	(shoulder)		
Tris:Ni 3, 80 °C	–	674	833		1020	1380		3300	
		656			1070	1580		3360	
Ni control, 80 °C	–	620	831	988	1050	1370	1620	3300	
Tris:Co 3, 80 °C	–	717	834	975	1070	1350			3370
		742	858			1540			3490
Co control, 80 °C	515	658	835	960	1070	1340			3380
		696				1540			3500
		766							
		805							
Tris:Fe 3, 80 °C	–	735	856		1080	1380			
Fe control, 80 °C	541	670	811		1090	1380			3490
			858			1560			
Metal mixtures									
Ni Tris, 25C	577	708	804		1030	1390	1650	3290	
					1100		(shoulder)		
Tris:Fe + Ni 3, 25 °C	573	632 (shoulder)	801		1020	1370	1650	3220	
					1070	1480	(shoulder)		
Co Tris, 25C	552	688	830	954	1080	1390	1660 (shoulder)		3500
Tris:Fe + Co 3, 25 °C	580	660	828		1080	1380		3380	
		697 (shoulder)				1480 (shoulder)			
Fe Tris, 25C	533	666	820		1090	1370		3180	3490
		700 (shoulder)				1540			
Ni Tris, 80C		661	829		1010	1390	1610	3330	
					1080	1470 (shoulder)			
no Tris, Fe + Ni, 80C	527	647	836	944		1360		3380	3490
		693				1540			
Tris:Fe + Ni 3, 80C	527	652	859		1030	1380		3310	
		685			1080	1470			
		740			(shoulder)	(shoulder)			
Co Tris, 80C	519	671	832	977	1060	1350			3390
		705				1480			3510
Tris:Fe + Co 3, 80C	543	669	830	930	1080	1380			3470
		705				1550			
Fe Tris, 80C	538	670	811		1010	1380		3290	3480
					1090 (shoulder)	1570			

of the metal-amine bond. For Fe, the Tris base Fe mixture precipitates green rust ($Fe(II)_3Fe(III)(OH^-)_8^+ \cdot Cl^- \cdot nH_2O$), precluding its use for these experiments. The difference between using Tris-HCl over Tris buffer at 80 °C was found to be negligible, thus only Tris buffer is reported. At 80 °C, the strength of the Ni-Tris complex is greater than the Co-Tris complex, although the effect is less than at lower temperature, and no excess Fe is observed relative to the control (Fig. 8b).

The rate of solid carbonate precipitation from the apparent Tris-bound metal is also 2nd order with respect to the metal concentration for both Ni and Co. The linear slope in 2nd order rates as a function of $1/[Tris]_0$ gives the Tris-dependent rate constant for the disjunctive pathway (e.g., reaction 11, using Ni as an example) and the intercept gives the Tris-dependent rate constant for the adjunctive pathway (reaction 12). For carbonate precipitation from Ni and Co bound to Tris at 25 °C, there is effectively no contribution from the adjunctive pathway (Fig. 8c). The rate of metal lost due to carbonate precipitation following the disjunctive pathway of the Tris-HCl complexed metal at 25 °C is nearly identical for Ni ($k = 5e^{-5}\ M^{-1}s^{-1}$) and Co ($k = 9e^{-5}\ M^{-1}s^{-1}$), but and order of magnitude slower for Ni bound to Tris base ($k = 2e^{-4}\ M^{-1}s^{-1}$) than Co ($k = 1e^{-3}\ M^{-1}s^{-1}$) (Fig. 8c). The inconsistency in k_{excess} for the Fe experiments, which may stem from inconsistencies in the amorphous iron carbonate that precipitated, prevent any conclusions concerning pathway or rates. We hypothesize that slight changes in the stoichiometry of this phase, which is more like a hydrated chukanovite phase than a hydrous carbonate phase, caused the variability observed.

The rate of carbonate precipitation of complexed Ni at 80 °C also follows a disjunctive pathway ($k = 3.6e^{-3}\ M^{-1}s^{-1}$) and is slower than the rates of complexed Co (Fig. 8d). However, the rates of complexed Co do not follow a linear trend, which can result from shift in mineralogy from a rosasite-like phase to an amorphous carbonate phase as the amount of Tris-bound Co increases (Fig. 5e–h, 7b). More complexation decreases the rate of Co carbonate precipitation, forming more pure carbonate minerals. Presumably the same pattern exists for Tris-bound Fe(II), based on the mineralogy observed, although the rates at these conditions are so rapid at 80 °C that they cannot be quantified. These observations are consistent with solubility constants for the rosasite family of minerals being higher than the corresponding carbonate minerals (Table 2), suggesting the apparent relative solubilities of rosasite and carbonate are strongly affected by the abundance of complexed metal ions.

4.3. Effect of environmental variables on carbonate precipitation

Environmental factors, such as pH, temperature, and mixed metal solutions, are important to constrain to enable a predictive understanding of metal mobility in carbonate-rich systems, whether these are

Table 2
Stability constants for relevant reactions at 25 °C and 80 °C, I = 0 unless otherwise noted.

$(HOCH_2)_3CNH_2$ defined as L
$(HOCH_2)_3CNH_3^+$ defined as HL^+
$(OCH_2)(HOCH_2)_2CNH_2^-$ defined as $H_{-1}L^-$
$(OCH_2)_2(HOCH_2)CNH_2^{2-}$ defined as $H_{-2}L^{2-}$

	logK (25°C)	log K (80°C)
(1) $HL^+ = L + H^+$	−8.08[d]	−6.82[d]
(2) $HCO_3^- = CO_3^{2-} + H^+$	−9.68[g]	−9.25[g]
(3) $H_2CO_{3(aq)} = HCO_3^- + H^+$	−6.15[g]	−6.05[g]
(4) $Ni^{2+} + L = NiL^{2+}$	2.63[e]	
(5) $NiL^{2+} + L = NiL_2^{2+}$	1.9[e]	
(6) $2Ni^{2+} + 3L = Ni_2(H_{-1}L)_3^+ + 3H^+$	−13.4[e]	
(7) $3Ni^{2+} + 3L = Ni_3(H_{-2}L)_2(H_{-1}L)^+ + 5H^+$	−27.0[e]	
(8) $Co^{2+} + L = CoL^{2+}$	2.18[k]	
(9) $2Co^{2+} + 2L = (Co(H_{-1}L)^+)_2 + 2H^+$[f]		
(10) $Fe^{3+} + 2L = Fe(L)(H_{-1}L)^{2+} + H^+$[f]		
(11) $NiL^{2+} = Ni^{2+} + L + CO_3^{2-} = NiCO_{3(aq)} + L + 6H_2O = NiCO_3{*}6H_2O_{(s)}$		
(12) $NiL^{2+} + CO_3^{2-} = LNiCO_{3(aq)} = NiCO_{3(aq)} + L + 6H_2O = NiCO_3{*}6H_2O_{(s)}$		
(13) $Ni^{2+} + CO_3^{2-} = NiCO_{3(aq)}$	4.83[a]	3.94[a]
(14) $Co^{2+} + CO_3^{2-} = CoCO_{3(aq)}$	4.41[a]	4.16[a]
(15) $Fe^{2+} + CO_3^{2-} = FeCO_{3(aq)}$	4.73[a]	4.64[a]
(16) $Ni^{2+} + HCO_3^- = NiHCO_3^+$	2.22[a]	2.96[a]
(17) $Co^{2+} + HCO_3^- = CoHCO_3^+$	2.20[a]	2.88[a]
(18) $Fe^{2+} + HCO_3^- = FeHCO_3^+$	2.17[a]	3.85[a]
(19) $Ni^{2+} + CO_3^{2-} + 6H_2O = NiCO_3{*}6H_2O_{(s)}$	10.64[b]	10.64[b]
(20) $Co^{2+} + CO_3^{2-} = CoCO_{3(s)}$	9.98[j]	
(21) $2Co^{2+} + CO_3^{2-} + 2OH^- + H_2O = CoCO_3{*}Co(OH)_2{*}H_2O_{(s)}$	30.3[c]	
(22) $2Fe^{2+} + CO_3^{2-} + 2OH^- + H_2O = FeCO_3{*}Fe(OH)_2{*}H_2O_{(s)}$	16.2[i]	
(23) $2Fe^{2+} + HCO_3^- + 2H_2O = FeCO_3{*}Fe(OH)_{2(s)} + 3H^+$	10.24[h]	
(24) $2Fe^{2+} + CO_3^{2-} = FeCO_{3(s)}$		

[a] Fouillac and Criaud (1984); 80 °C logK values calculated using the Van't Hoff equation.
[b] Wallner et al. (2002).
[c] González-López et al., 2018, I = 0.025.
[d] Bates and Hetzer (1961); 80 °C logK values calculated using eq. 3 in Bates and Hetzer (1961).
[e] Bai and Martell (1969), I = 0.1.
[f] inferred reaction from Dotson (1972).
[g] Millero (2010) (logK of pure water adjusted for temperature and salinity for this study using eqs 16–21 in Millero, 2010).
[h] Singer and Stumm (1970).
[i] Kim et al. (2017).
[j] Smith et al., 1976; Naumov et al. (1974) from Riechers et al. (2022).
[k] Hanlon et al. (1966), I = 0.6.

engineered or natural systems. The apparent solubility of metal carbonate decreases as more metal is complexed to Tris and the Tris complex selectively binds Ni > Co > Fe at 25 °C (Fig. 2a–c). In addition, the rate of Tris-carbonate ligand exchange is selective, with Co > Ni (Fig. 8c). The strength of the complex is higher when it is formed in slightly acidic conditions (pH ~ 5) than neutral conditions, as observed in both the amount and rate of precipitation, with a greater impact of pH on Co than Ni (Fig. 8a–c). This pattern was also observed when the pH of the carbonate-buffered solution was raised, which had a minimal impact on complexed Ni but a large impact of complexed Co and Fe (Fig. 3c). This is consistent with the difference in bonding environment between the expected Ni complexes (e.g., NiL_2^{+2} or $Ni(H_{-1}L)(L)^+$ at pH 8) and Co complex (e.g., $(Co(H_{-1}L)^+)_2$), suggesting the high spin five-coordinate Co complex with a trigonal bipyramidal structure is weaker in a carbonate-rich system. Our data also suggest the Fe(II) complex shares a greater similarity to the structure of the Co(II) complex than the Ni(II) complex, although this has not been confirmed (to our knowledge) in the literature. Given the similarity in amorphous carbonate minerals produced from solutions of Ni, Co, and Fe complexes (Figs. 5 and 7), it therefore seems likely that ligand exchange and the difference in the nature of the complexes can explain the observations rather than mineral solubility. In fact, the calculated saturation indices of hellyerite is almost invariant as pH shifts from 8 to 10.5 (3.30–3.31 with a maximum at pH 9 at 25 °C and 3 mM Ni) and saturation of sphaerocobaltite changes only slightly (2.93–3.24 with a maximum at pH 10 at 25 °C and 3 mM Co). Chukanovite saturation indices is the most affected by pH, shifting from 30.45 to 34.82 at 25 °C and 3 mM Fe. These observations persist at 80 °C, with Tris selectively binding Ni ≫ Co at Tris:Me ratios >1 (Fig. 8b) and selective rates of Tris-carbonate exchange for Ni > Co (Fig. 8d). In contrast to 25 °C, the carbonate phase precipitated was altered as a function of the Tris:Me complex for Co and Fe but not for Ni (Figs. 5 and 7), with a transition towards purer crystalline carbonate (sphaerocobaltite or siderite) with increasing complexation. The calculated saturation indices at 80 °C, however, predicts a higher

Table 3
UV–Vis bands and estimated octahedral field splitting (Δ_0) for Ni and Co Tris complexes shown in Fig. 1. Estimated overall stabilization energy (SE) assumes a high spin complex and an average value for the pairing energy of 20,000 cm^{-1}.

	λ(nm)	Δ_0 (cm^{-1})	SE (cm^{-1})
Ni-Tris-HCl	394	25381	29543
pH 4.6	661	15129	41846
	725	13793	43448
Ni-Tris base	385	25974	28831
1:1 or (3:1)	651 (631)	15361 (15848)	41567 (40983)
pH 7.9 (8.4)			
Co-Tris-HCl	478	20921	23264
pH 5.1–5.6	515	19417	24466
Co-Tris buffer	256	39063	8750
pH 8.1–8.3	434	23041	21567
	477	20964	23229
Ni + Fe-Tris-HCl	377	26525	28170
pH 5.3			
Co + Fe-Tris-HCl	450	22222	22222
pH 4.9	494	20243	23806

supersaturation for the hydrated or hydroxycarbonate phases than the pure carbonate phases: 16.5 for the hydrated hellyerite over 11.9 for pure gaspeite, 51.29 for the hydroxycarbonate rosasite over 14.1 for the pure sphaerocobaltite, and 34.9 for the hydroxycarbonate chukanovite over 5.1 for pure siderite This suggests that at 80 °C, the ligand exchange mechanism affects not only the amount and rate of carbonate precipitation but also strongly affects the mineral phase produced, promoting thermodynamically less favorable pure carbonate phases, and therefore also the potential incorporation of other metals present in solution.

In Fe–Ni mixtures, the amount of Ni carbonate precipitation is lower relative to Ni-only reactions at both 25 °C and 80 °C (Fig. 4b). The same is true for Co at both 25 °C and 80 °C (Fig. 4c). Both Ni and Co increase the amount of Fe carbonate precipitation, with the effect of Ni much greater than Co at 25 °C (Fig. 4d). Combining these observations at 25 °C reveals a generalizable shift from more total precipitation (negative values) to less total precipitation (positive values) as the Tris:metal ratio increases (Fig. 4d). This is primarily due to more Ni/Co precipitation in the absence of Tris, less Fe precipitation at Tris:Me of 3, and a mixture of both processes at Tris:Me of 1 (Fig. 4d). This suggests the apparent solubility of Co and Ni is decreased in metal mixtures relative to single metal solutions, with Fe affecting Ni more than Co (Fig. 4d). As the Tris:Me ratio increases, the presence of Ni or Co has an apparent stabilizing effect on Fe in the complex, inhibiting precipitation of all metal carbonate. The Tris:Me ratio at which the effect of increased solubility of Fe is balanced by the decreased solubility of Ni or Co is ~1.8 for Ni and ~1.6 for Co (Fig. 4d, dashed lines), which is consistent with larger discrepancy and weaker bonding of Ni in the mixed Fe–Ni–Tris than the single metal Ni complex (a difference of 1373 cm^{-1}) relative to the discrepancy in bonding of Co in the Fe–Co–Tris relative to the single metal Co complex (a difference of 660 and 1041 cm^{-1}) indicated by the UV–Vis spectra (Table 3). Carbonate mineralogy is not affected by the degree of complexation at 25 °C (Fig. 6a and b and 7c,d) and the distribution of Fe:Co and Fe:Ni is slightly higher for Co than Ni (2.4 vs. 2.1, respectively) according to EDS analysis, which is consistent with the fluid chemistry (Fig. 4d). As with the single metal experiments at 80 °C, the mixed metal experiments produced multiple mineral morphologies but only in the Fe–Ni mixture and not in the Fe–Co mixture, in contrast to the single metal experiments. With increasing Tris complexation, the more crystalline morphologies (rods and spheres, respectively) partitioned Fe preferentially (Fe:Ni ~ 5.7), while Ni increasingly partitioned into the plate-like phase (Fe:Ni ~ 2.8 and 1.1 with increasing Tris:Me) and the residual matrix became increasingly enriched in Ni (1.7 and 0.8 with increasing Tris:Me). In addition, Tris more effectively selectively binds metals following the order Ni > Co > Fe in the Fe:Ni mixtures than in single metal solutions. These observations have implications for trace metal mobility in alkaline solutions at slightly elevated temperatures in systems where relatively simple bidentate primary amine organic compounds are present.

In general, the selectivity of Tris for Ni(II) and Co(II) over Fe(II) during carbonate precipitation from alkaline solutions is enhanced at lower temperature (25 °C) and lower pH (~8), although the carbonate produced is a hydrated nanocrystalline metastable phase. Increasing

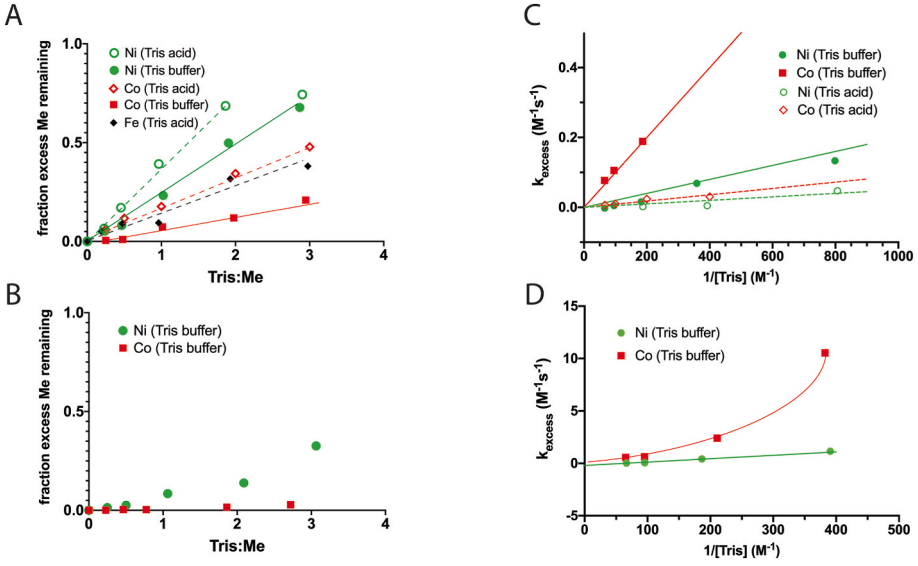

Fig. 8. (A) Fraction of excess metal (bound) remaining in solution after 5 h at 25 °C for Ni (green), Co (red), and iron (black) for variable Tris:metal ratios. The effect of using Tris buffer (closed symbols, solid lines) or Tris acid (open symbols, dashed lines) is also shown. (B) Fraction of excess metal remaining in solution after 5 h at 80 °C using the same symbols as in (A). (C) Conditional 2nd order rate constants for carbonate precipitation of the Ni and Co bound to Tris acid or Tris buffer (i.e., excess metal) at 25 °C. (D) Conditional 2nd order rate constants for carbonate precipitation of the Ni and Co bound to Tris at 80 °C. (For interpretation of the references to color in this figure legend, the reader is referred to the Web version of this article.)

temperature to 80 °C stabilizes the more thermodynamically favorable hydrated minerals of the rosasite family ($Me_2CO_3(OH)_2{\cdot}H_2O$) for Co(II) and Fe(II) at pH 8; however, increased Tris complexation promotes precipitation of more pure carbonate phases and leads to larger crystal size. In mixed metal solutions (Fe–Ni and Fe–Co) that are more realistic for both engineered and natural systems, the presence of Fe(II) the precipitation of Ni(II) and Co(II) is increased. With increasing Tris complexation, less total metal precipitates and at 80 °C promotes greater partitioning of Ni(II) into a separate carbonate phase with distinct morphology from Fe(II). These results have the potential to improve efficiency of critical element (Ni and Co) recovery from Fe-rich source materials while promoting carbon sequestration using Tris directly in engineered systems. For example, successful protocols for indirect mineral carbon sequestration in which the cations leached from silicates are subsequently precipitated as carbonates from solution (e.g., Bobicki et al., 2014; Park and Fan, 2004; Teir et al., 2007) overlap the optimal conditions for selective complexation of metals using Tris and may be improved by utilizing similar amine-bearing bidentant ligands. It is also possible that during direct silicate carbonation utilizing high p_{CO2} conditions (up to 20 MPa; Prigiobbe and Mazzotti, 2011; Bonfils et al., 2012; Krevor and Lackner, 2009; Bobicki et al., 2015), which has been tested primarily for efficiency of magnesium carbonate conversion of mafic silicates, metal-selective ligands such as Tris can be implemented to promote critical element concentration in the leachate. These results also have implications in carbonate-rich natural systems where organic compounds similar to Tris that can form bidentate mixed amine/alcohol complexes (e.g., amino acids) may be important for regulating metal mobility and bioavailability.

5. Conclusions

Predicting the mobility of transition metal critical elements (e.g., Ni and Co) in the presence of organic ligands at carbonate-saturation conditions requires an understanding of how ligand-metal complexation impacts mineral solubility in both natural and industrial environments. In this study we evaluate the effect of Tris on metal complexation and carbonate precipitation under alkaline conditions (pH 8–10.5) at 25 °C and 80 °C in both single metal and mixed metal solutions to aid in the predictive understanding of how primary amine ligands impact metal mobility. Tris forms a stronger complex and is increasingly selective for trace metals with Ni(II) > Co(II) > Fe(II) during carbonate precipitation, with the rates decreasing but selectivity increasing at lower temperature and lower pH. Increased temperature results in a shift from metastable amorphous hydrated carbonates to a more crystalline mixture of rosasite-group minerals ($Co_2CO_3(OH)_2(H_2O)$ and $Fe_2CO_3(OH)_2$) and pure carbonates (sphaerocobaltite and siderite), with the latter more stabilized with increasing Tris complexation. The ligand exchange mechanism affects not only the amounts and rates of carbonate precipitation, but also strongly affects the mineral phase produced and, therefore, the potential incorporation efficiency of other metals present. In mixed metal solutions, the addition of Fe increases the amount of Ni and Co carbonate precipitation, while the presence of Ni and Co does not affect Fe carbonate precipitation. However, with increasing Tris concentrations, Ni and Co stabilize Fe complexation increasing the apparent solubility of all metal. Together these results aid in our understanding of the comparative impact of metal-organic ligand complexes on metal carbonate precipitation as a function of pH, temperature, ligand/metal ratio, and the diversity of metals present.

CRediT authorship contribution statement

J.L. Houghton: Writing – review & editing, Writing – original draft, Visualization, Methodology, Formal analysis, Conceptualization. **J.M. Haywood:** Writing – review & editing, Validation, Methodology, Conceptualization. **Y. Wang:** Writing – review & editing, Investigation. **Y.S. Jun:** Writing – review & editing, Funding acquisition. **D.A. Fike:** Writing – review & editing, Supervision, Funding acquisition.

Declaration of competing interest

The authors declare that they have no known competing financial interests or personal relationships that could have appeared to influence the work reported in this paper.

Acknowledgements

This work was supported by the U.S. Department of Energy, Office of Science, Office of Basic Energy Sciences, Chemical and Materials Sciences to Advance Clean Energy Technologies and Low-Carbon Manufacturing (DE-SC0023390).

Appendix A. Supplementary data

Supplementary data to this article can be found online at https://doi.org/10.1016/j.apgeochem.2025.106512.

Data availability

Data will be made available on request.

References

Azoulay, I., Rémazeilles, C., Refait, P., 2012. Determination of standard Gibbs free energy of formation of chukanovite and pourbaix diagrams of iron in carbonated media. Corros. Sci. 58, 229–236.
Bai, K.S., Martell, A.E., 1969. The interaction of 2-amino-2-(hydroxymethyl)-1, 3-propanediol with copper (II) and nickel (II) ions. J. Inorg. Nucl. Chem. 31 (6), 1697–1707.
Bates, R.G., Hetzer, H.B., 1961. Dissociation constant of the protonated acid form of 2-amino-2-(hydroxymethyl)-1, 3-propanediol [tris-hydroxymethyl)-aminomethane] and related thermodynamic quantities from 0 to 50. J. Phys. Chem. 65 (4), 667–671.
Baxter, L.A., Bobrowski, A., Bond, A.M., Heath, G.A., Paul, R.L., Mrzljak, R., Zarebski, J., 1998. Electrochemical and spectroscopic investigation of the reduction of dimethylglyoxime at mercury electrodes in the presence of cobalt and nickel. Anal. Chem. 70 (7), 1312–1323.
Bethke, C.M., 2022. Geochemical and Biogeochemical Reaction Modeling. Cambridge university press.
Bette, S., Rincke, C., Dinnebier, R.E., Voigt, W., 2016. Crystal structure and hydrate water content of synthetic hellyerite, NiCO3· 5.5 H2O. Z. Anorg. Allg. Chem. 642 (9-10), 652–659.
Bobicki, E.R., Liu, Q., Xu, Z., 2014. Ligand-promoted dissolution of serpentine in ultramafic nickel ores. Miner. Eng. 64, 109–119.
Bobicki, E.R., Liu, Q., Xu, Z., 2015. Mineral carbon storage in pre-treated ultramafic ores. Miner. Eng. 70, 43–54.
Bonfils, B., Julcour-Lebigue, C., Guyot, F., Bodénan, F., Chiquet, P., Bourgeois, F., 2012. Comprehensive analysis of direct aqueous mineral carbonation using dissolution enhancing organic additives. Int. J. Greenh. Gas Control 9, 334–346.
Dideriksen, K., Frandsen, C., Bovet, N., Wallace, A.F., Sel, O., Arbour, T., et al., 2015. Formation and transformation of a short range ordered iron carbonate precursor. Geochem. Cosmochim. Acta 164, 94–109.
Dotson, R.L., 1972. Characterization and studies of some four, five and six coordinate transition and representative metal complexes of tris-(hydroxymethyl)-aminomethane. J. Inorg. Nucl. Chem. 34 (10), 3131–3138.
Drever, J.I., Stillings, L.L., 1997. The role of organic acids in mineral weathering. Colloids Surf. A Physicochem. Eng. Asp. 120 (1–3), 167–181.
Dufaud, F., Martinez, I., Shilobreeva, S., 2009. Experimental study of Mg-rich silicates carbonation at 400 and 500 C and 1 kbar. Chem. Geol. 265 (1–2), 79–87.
Effenberger, H., Mereiter, K., Zemann, J., 1981. Crystal structure refinements of magnesite, calcite, rhodochrosite, siderite, smithonite, and dolomite, with discussion of some aspects of the stereochemistry of calcite type carbonates. Z. Kristallogr. Cryst. Mater. 156 (1–4), 233–244.
Fangueiro, D., Bermond, A., Santos, E., Carapuça, H., Duarte, A., 2002. Heavy metal mobility assessment in sediments based on a kinetic approach of the EDTA extraction: search for optimal experimental conditions. Anal. Chim. Acta 459 (2), 245–256.
Fouillac, C., Criaud, A., 1984. Carbonate and bicarbonate trace metal complexes: critical reevaluation of stability constants. Geochem. J. 18 (6), 297–303.
Frost, R.L., Wain, D.L., Martens, W.N., Reddy, B.J., 2007. Vibrational spectroscopy of selected minerals of the rosasite group. Spectrochim. Acta Mol. Biomol. Spectrosc. 66 (4–5), 1068–1074.
Gerdemann, S.J., O'Connor, W.K., Dahlin, D.C., Penner, L.R., Rush, H., 2007. Ex situ aqueous mineral carbonation. Environ. Sci. Technol. 41 (7), 2587–2593.

Gogol, D.B., Makasheva, A.M., Sadyrbekov, D.T., Dyussembayeva, L.F., Rozhkovoy, I.E., Ishmiev, I.I., et al., 2024. Evaluation of solubility and thermodynamic properties of synthetic nickel hydroxide carbonate. J. Solut. Chem. 1–11.
González-López, J., Fernández-González, Á., Jiménez, A., 2018. Precipitation behaviour in the system Ca2+-Co2+-CO32−-H2O at ambient conditions—Amorphous phases and CaCO3 polymorphs. Chem. Geol. 482, 91–100.
Grandstaff, D.E., 1986. The dissolution rate of forsteritic olivine from Hawaiian beach sand. Rates of chemical weathering of rocks and minerals.
Grauer, R., Berner, U., 1999. Solubility Products of M (II)-carbonates.
Hall, J.L., Swisher, J.A., Brannon, D.G., Liden, T.M., 1962. Copper (II) ion and nickel (II) ion complexes with 2-Amino-2-(hydroxymethyl)-1, 3-propanediol. Reactions with sodium hydroxide. Inorg. Chem. 1 (2), 409–413.
Hamilton, J.L., Wilson, S.A., Morgan, B., Harrison, A.L., Turvey, C.C., Paterson, D.J., Dipple, G.M., Southam, G., 2020. Accelerating mineral carbonation in ultramafic mine tailings via direct CO_2 reaction and heap leaching with potential for base metal enrichment and recovery. Econ. Geol. 115, 303–323.
Hänchen, M., Prigiobbe, V., Storti, G., Seward, T.M., Mazzotti, M., 2006. Dissolution kinetics of fosteritic olivine at 90–150 C including effects of the presence of CO2. Geochem. Cosmochim. Acta 70 (17), 4403–4416.
Hanlon, D.P., Watt, D.S., Westhead, E.W., 1966. The interaction of divalent metal ions with tris buffer in dilute solution. Anal. Biochem. 16 (2), 225–233.
Huang, C.K., Kerr, P.F., 1960. Infrared study of the carbonate minerals. Am. Mineral.: Journal of Earth and Planetary Materials 45 (3–4), 311–324.
Huang, W.H., Keller, W.D., 1972. Organic acids as agents of chemical weathering of silicate minerals. Nat. Phys. Sci. (Lond.) 239 (96), 149–151.
Hummel, W., Curti, E., 2003. Nickel aqueous speciation and solubility at ambient conditions: a thermodynamic elegy. Monatshefte für Chemie/Chemical Monthly 134, 941–973.
Hunt, A.J., Matharu, A.S., King, A.H., Clark, J.H., 2015. The importance of elemental sustainability and critical element recovery. Green Chem. 17 (4), 1949–1950.
Jiang, C.Z., Tosca, N.J., 2019. Fe (II)-carbonate precipitation kinetics and the chemistry of anoxic ferruginous seawater. Earth Planet Sci. Lett. 506, 231–242.
Jiang, C.Z., Tosca, N.J., 2020. Growth kinetics of siderite at 298.15 K and 1 bar. Geochem. Cosmochim. Acta 274, 97–117.
Jillot, B.A., Williams, R.J.P., 1958. 82. Further complexes of ferrous dimethylglyoxime. J. Chem. Soc. 462–467.
Katsikopoulos, D., Fernández-González, Á., Prieto, A.C., Prieto, M., 2008. Co-crystallization of Co (II) with calcite: implications for the mobility of cobalt in aqueous environments. Chem. Geol. 254 (1–2), 87–100.
Khan, S., Wani, O.B., Shoaib, M., Forster, J., Sodhi, R.N., Boucher, D., Bobicki, E.R., 2021. Mineral carbonation for serpentine mitigation in nickel processing: a step towards industrial carbon capture and storage. Faraday Discuss. 230, 172–186.
Kim, S., Marrs, C., Nemer, M., Je-Hun Jang, J., 2017. Solubility model for ferrous iron hydroxide, hibbingite, siderite, and chukanovite in high saline solutions of sodium chloride, sodium sulfate, and sodium carbonate. ACS Earth Space Chem. 1 (10), 647–663.
Kohls, D.W., Rodda, J.L., 1966. Gaspeite,(Ni, Mg, Fe)(CO3), a new carbonate from the gaspé Peninsula, Quebec. Am. Mineral.: Journal of Earth and Planetary Materials 51 (5–6), 677–684.
Kondratenko, Y.A., Nikonorova, A.A., Zolotarev, A.A., Arsent'ev, M.Y., Nyanikova, G.G., Ugolkov, V.L., et al., 2022. Synthesis, structure and properties of tris (hydroxymethyl) aminomethane complexes with biogenic metal salts. Inorg. Chim. Acta. 530, 120705.
Krevor, S.C., Lackner, K.S., 2009. Enhancing process kinetics for mineral carbon sequestration. Energy Proc. 1 (1), 4867–4871.
Kursunoglu, S., Kaya, M., 2015. Dissolution behavior of Caldag lateritic nickel ore subjected to a sequential organic acid leaching method. Int. J. Miner. Metall. Mater. 22, 1131–1140.
Lambart, S., Hamilton, S., Lang, O.I., 2022. Compositional variability of San Carlos olivine. Chem. Geol. 605, 120968.
Lazo, D.E., Dyer, L.G., Alorro, R.D., 2017. Silicate, phosphate and carbonate mineral dissolution behaviour in the presence of organic acids: a review. Miner. Eng. 100, 115–123.
Leite, H.M., Moya, H.D., Coichev, N., Neves, E.A., 2000. The interaction of 2-amino-2-hydroxymethyl-1, 3-propanediol with cobalt (II) and manganese (II) ions. J. Coord. Chem. 49 (3), 251–259.
Ma, F., Jagner, D., Renman, L., 1997. Mechanism for the electrochemical stripping reduction of the nickel and cobalt dimethylglyoxime complexes. Anal. Chem. 69 (9), 1782–1784.
Martell, A.E., Smith, R.M., Motekaitis, R.J., 1993. NIST Critical Stability Constants of Metal Complexes Data Base (Computerized).
Matus, C., Stopic, S., Etzold, S., Kremer, D., Wotruba, H., Dertmann, C., Telle, R., Friedrich, B., Knops, P., 2020. Mechanism of nickel, magnesium, and iron recovery from olivine bearing ore during leaching with hydrochloric acid including a carbonation pre-treatment. Metals 10, 811.
Millero, F.J., 2010. Carbonate constants for estuarine waters. Mar. Freshw. Res. 61 (2), 139–142.
Nagaj, J., Stokowa-Sołtys, K., Kurowska, E., Fraczyk, T., Jeżowska-Bojczuk, M., Bal, W., 2013. Revised coordination model and stability constants of Cu (II) complexes of tris buffer. Inorg. Chem. 52 (24), 13927–13933.
Naumov, V.B., Khakimov, A.K.H., Khodakovskiy, I.L., 1974. Solubility of carbon dioxide in concentrated chloride solutions at high temperatures and pressures. Geochem. Int. 11, 31–41.
Nieboer, E., Richardson, D.H., 1980. The replacement of the nondescript term 'heavy metals' by a biologically and chemically significant classification of metal ions. Environ. Pollut. Ser. B Chem. Phys. 1 (1), 3–26.
Olsen, A.A., Rimstidt, J.D., 2008. Oxalate-promoted forsterite dissolution at low pH. Geochem. Cosmochim. Acta 72 (7), 1758–1766.
Park, A.H.A., Fan, L.S., 2004. CO2 mineral sequestration: physically activated dissolution of serpentine and pH swing process. Chem. Eng. Sci. 59 (22–23), 5241–5247.
Prigiobbe, V., Mazzotti, M., 2011. Dissolution of olivine in the presence of oxalate, citrate, and CO2 at 90 C and 120 C. Chem. Eng. Sci. 66 (24), 6544–6554.
Rémazeilles, C., Refait, P., 2009. Fe (II) hydroxycarbonate Fe2 (OH) 2CO3 (chukanovite) as iron corrosion product: synthesis and study by Fourier transform infrared spectroscopy. Polyhedron 28 (4), 749–756.
Riechers, S.L., Ilton, E.S., Qafoku, O., Du, Y., Kerisit, S.N., 2022. Cobalt hydroxide–cobalt carbonate competitive growth on carbonate surfaces. Chem. Geol. 605, 120951.
Saito, M.A., Moffett, J.W., 2001. Complexation of cobalt by natural organic ligands in the Sargasso Sea as determined by a new high-sensitivity electrochemical cobalt speciation method suitable for open ocean work. Mar. Chem. 75 (1–2), 49–68.
Sarker, S.K., Haque, N., Bhuiyan, M., Bruckard, W., Pramanik, B.K., 2022. Recovery of strategically important critical minerals from mine tailings. J. Environ. Chem. Eng. 10 (3), 107622.
Senior, G.D., Thomas, S.A., 2005. Development and implementation of a new flowsheet for the flotation of a low grade nickel ore. Int. J. Miner. Process. 78 (1), 49–61.
Singer, P.C., Stumm, W., 1970. The solubility of ferrous iron in carbonate-bearing waters. J. Am. Water Works Assoc. 62 (3), 198–202.
Sissmann, O., Daval, D., Brunet, F., Guyot, F., Verlaguet, A., Pinquier, Y., et al., 2013. The deleterious effect of secondary phases on olivine carbonation yield: insight from time-resolved aqueous-fluid sampling and FIB-TEM characterization. Chem. Geol. 357, 186–202.
Smith, R.M., Martell, A.E., Smith, R.M., Martell, A.E., 1976. Inorganic ligands. Critical Stability Constants: Inorganic Complexes, pp. 1–129.
Snæbjörnsdóttir, S.Ó., Sigfússon, B., Marieni, C., Goldberg, D., Gislason, S.R., Oelkers, E. H., 2020. Carbon dioxide storage through mineral carbonation. Nat. Rev. Earth Environ. 1 (2), 90–102.
Stoilova, D., Koleva, V., Vassileva, V., 2002. Infrared study of some synthetic phases of malachite (Cu2 (OH) 2CO3)–hydrozincite (Zn5 (OH) 6 (CO3) 2) series. Spectrochim. Acta Mol. Biomol. Spectrosc. 58 (9), 2051–2059.
Stumm, W., Morgan, J.J., Drever, J.I., 1996. Aquatic chemistry. J. Environ. Qual. 25 (5), 1162.
Teir, S., Revitzer, H., Eloneva, S., Fogelholm, C.J., Zevenhoven, R., 2007. Dissolution of natural serpentinite in mineral and organic acids. Int. J. Miner. Process. 83 (1–2), 36–46.
Wallner, H., Preis, W., Gamsjäger, H., 2002. Solid–solute phase equilibria in aqueous solutions: XV [1]. Thermodynamic analysis of the solubility of nickel carbonates. Thermochim. Acta 382 (1–2), 289–296.
Wang, F., Giammar, D.E., 2013. Forsterite dissolution in saline water at elevated temperature and high CO2 pressure. Environ. Sci. Technol. 47 (1), 168–173.
Wang, F., Dreisinger, D., Jarvis, M., Hitchins, T., Trytten, L., 2021. CO2 mineralization and concurrent utilization for nickel conversion from nickel silicates to nickel sulfides. Chem. Eng. J. 406, 126761.
Weir, C.E., Lippincott, E.R., 1961. Infrared studies of aragonite, calcite, and vaterite type structures in the borates, carbonates, and nitrates. Journal of Research of the National Bureau of Standards. Section A, Physics and Chemistry 65 (3), 173.
White, W.B., 1974. The carbonate minerals. In: Farmer, V.C. (Ed.), The Infrared Spectra of Minerals, Mineralogical Society Monograph, vol. 4.
Wogelius, R.A., Walther, J.V., 1991. Olivine dissolution at 25 C: effects of pH, CO2, and organic acids. Geochem. Cosmochim. Acta 55 (4), 943–954.
Zhang, H., Van Den Berg, C.M., Wollast, R., 1990. The determination of interactions of cobalt (II) with organic compounds in seawater using cathodic stripping voltammetry. Mar. Chem. 28 (4), 285–300.